

SUITABILITY OF SHAPE MEMORY ALLOYS FOR VIBRATION ISOLATION
WITH APPLICATION TO LAUNCH VEHICLE PAYLOADS

A Thesis

by

JOHN JERAMY MAYES

Submitted to the Office of Graduate Studies of
Texas A&M University
in partial fulfillment of the requirements for the degree of
MASTER OF SCIENCE

December 2001

Major Subject: Aerospace Engineering

SUITABILITY OF SHAPE MEMORY ALLOYS FOR VIBRATION ISOLATION
WITH APPLICATION TO LAUNCH VEHICLE PAYLOADS

A Thesis

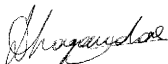
by

JOHN JERAMY MAYES


Submitted to Texas A&M University
in partial fulfillment of the requirements
for the degree of

MASTER OF SCIENCE

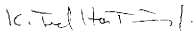
Approved as to style and content by:



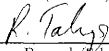
Dimitris C. Lagoudas
(Chair of Committee)



Thomas C. Pollock
(Member)



K. Ted Hartwig
(Member)



Ramesh Talreja
(Head of Department)

December 2001

Major Subject: Aerospace Engineering

ABSTRACT

*Suitability of Shape Memory Alloys for Vibration Isolation with
Application to Launch Vehicle Payloads. (December 2001)*

John Jeramy Mayes, B.S., Texas A&M University

Chair of Advisory Committee: Dr. Dimitris C. Lagoudas

This work details an investigation into the suitability of Shape Memory Alloys for the task of vibration isolation based on the similarities between the Shape Memory Alloy pseudoelastic behavior and the softening response of isolators whose response is similar to a buckling elastomer. In this work, a simplified material model for the prediction of the non-linear, hysteretic nature of the pseudoelastic force-displacement relationship is developed. This material model is coupled with the numerical simulation of a dynamic system whose restoring force is provided by Shape Memory Alloys, providing an efficient software tool for the modelling of such systems. A thorough experimental investigation is also presented in which the behavior of a prototype Shape Memory Alloy-based isolation device is explored. Numerous quasi-static tests are performed, as well as a comprehensive series of dynamic tests on the prototype device. Results of these tests are compared with the predictions of the numeric simulation. From this comparison, several important conclusions are drawn concerning the application of Shape Memory Alloys to vibrating systems. The most important conclusion is that in order for the non-linearity and hysteresis present in Shape Memory Alloys to be effective in reducing the transmissibility of a dynamic system, there must be large amplitude deflections in the system.

To Becky, for being my biggest champion and supporter throughout everything.

ACKNOWLEDGMENTS

The work presented here would not have been possible without the instruction and guidance of my advisor and committee chair, Dr. Dimitris C. Lagoudas, whose example of dedication and work ethic has been a wonderful example to me. Additionally, the financial support of the Air Force Office of Scientific Research and the Air Force Research Laboratory at Kirtland Air Force Base are greatly appreciated. A great deal of appreciation is also due to Dr. Tom Pollock, for both serving on my thesis committee and for providing valuable instruction and advice throughout both my graduate and undergraduate years. I would also like to thank Dr. Ted Hartwig for serving on my thesis committee and providing the objective viewpoint so often needed during graduate studies. Finally, I would like to give special thanks to Mughees Khan and Peter Popov, two friends who never failed to share their insight and knowledge when I needed assistance.

As with any journey such as this, I would have faltered and failed long ago without the support of the friends I have made along the way. A great deal of thanks goes to both David Miller and P.K. Imbric, who through their example, dedication, and tireless instruction, both in and out of the classroom, gave me the inspiration to begin this journey and the tools and knowledge to succeed. To these two men, I owe an incredible debt of gratitude. Thanks also to those friends created through the incessant pressures of graduate study, many of whom I am sure will continue to remain close friends long after the details of this journey fade. To Cale Stephens, Eric Vandygriff, Justin Strelec, Luke Penrod, Mughees Khan and the many others who have been there for the Saturday morning movies, the many lunches around the lab table and at Northgate, and the long discussions of research, but more importantly, life.

Finally, I would like to thank those “behind the scenes” individuals who can never receive enough thanks. To my parents, whose support, both emotionally and financially, is more than any child could ask. To my sister, who gave me never-ending support through this long journey. To Becky, whose love and faith in my abilities allowed me to get through the times when I thought I could not go on. And finally, Lona, the confidant, friend, and advocate to a generation of Aggie Grads, without whose support and advice I could not have even begun this task, much less completed it. These are the ones who deserve all the riches that life has to offer.

TABLE OF CONTENTS

CHAPTER		Page
I	INTRODUCTION	1
	A. Recent Work in Spacecraft Vibration Isolation	2
	B. Application of Shape Memory Alloys to Vibration Isolation	4
	C. Objective of This Work	5
II	SHAPE MEMORY ALLOY MATERIAL RESPONSE	7
	A. Shape Memory Alloys	7
	B. Modelling of Vibration Isolation with SMA	8
	C. Similarities Between Traditional Isolators and the Pseudo-elastic Behavior of SMAs	11
III	SIMPLIFIED SHAPE MEMORY ALLOY MATERIAL MODEL	13
	A. Determination of Material Force-Displacement Response	13
	B. Major Loop Loading	21
	C. Minor Loop Loading	23
	D. Characterization of SMA Tubular Springs	28
IV	DEVELOPMENT OF SMA VIBRATION EXPERIMENT	31
V	DEVELOPMENT OF NUMERICAL SIMULATION OF A VIBRATING SYSTEM WITH SMA SPRINGS	36
	A. Analysis of the Single Degree of Freedom Dynamic System	36
	B. Numerical Implementation of Solution to SDOF System with SMA Components	39
	C. Validation of Numerical Integration	42
	D. Investigation into the System Response of the Prototype SMA Based Isolation Device	46
	1. Numerical Prediction of System Response	46
	2. Experimental Investigation of System Response	48
	E. Simulation Results Based on Proposed Experiments	48
VI	EXPERIMENTAL RESULTS	62
	A. Vibration Testing of SMA Based Isolation Device	62

CHAPTER	Page
B. Results From Vibration Testing of SMA Based Isolation Device	68
1. Effect of Changes in Loading on System Response	68
2. Effect of Changes in SMA Spring Pre-Compression on System Response	74
VII COMPARISON OF EXPERIMENTAL RESULTS AND THEORY	82
VIII DISCUSSION OF RESULTS AND FUTURE WORK	88
A. Comments on the Differences Observed Between Experimental Results and Expected Performance	88
B. Future Work	89
IX CONCLUSIONS	91
REFERENCES	93
APPENDIX A	100
APPENDIX B	105
VITA	119

LIST OF FIGURES

FIGURE	Page
1	a) Stress vs. Temperature Graph Indicating Start and Finish of Transformation Between Austenite and Martensite Phases. b) Pseudoelastic Loading Response of SMA 9
2	Force vs. Displacement Response of Pseudoelastic SMA with K_M , K_A and δ_{max}^{tr} Labelled 14
3	Differential Scanning Calorimeter Results for SMA Material 15
4	SMA Force-Temperature-Phase Diagram with Pseudoelastic Loading Path 18
5	Simplified Pseudoelastic Force vs. Displacement Response of SMA for Major Loop Loading 19
6	Representative Displacement Path for Minor Loop Loading 24
7	Simplified Pseudoelastic Force vs. Displacement Response of SMA for Minor Loop Loading 25
8	Force vs. Displacement Response of SMA Tube Spring with Response from Simplified Pseudoelastic Model Showing Major and Minor Loop Response as Calibrated for This Work 30
9	Schematic of SMA Spring-Mass Isolation System as Designed 32
10	Various Schematics of SMA Spring-Mass Isolation System 34
11	Assembly of Vibration Isolation Experiment 35
12	Detail of SMA Tube Spring Mounting 35
13	a) Schematic of SMA Spring-Mass Isolation System. b) Free Body Diagram of SMA Spring-Mass Isolation System 38

FIGURE	Page
14	Flowchart of Algorithm Used to Calculate the Time History of the Dynamic System 41
15	Screen Captures of Vibration Isolation Numerical Simulation 43
16	Response of Linearized Spring-Mass System Calculated Using Newmark Method and Analytical Solution 44
17	Transmissibility for a Linear Spring-Mass System, Using Newmark Method and Analytical Solution 45
18	Individual Tube Spring and System Response for Pre-Compression of 30% of Tube Diameter 47
19	System Response for Various Levels of Pre-Compression at a Displacement Amplitude of $\pm 1 \text{ mm}$ 49
20	System Response for Various Amplitudes of Displacement at a Pre-compression Level of -2 mm 50
21	Quasi-Static Evaluation of the Force vs. Displacement Response of the Experimental System with Four SMA Tube Springs 51
22	Quasi-Static Evaluation of the Force vs. Displacement Response of the Experimental System with Six Tube Springs 52
23	Comparison of Experimental and Theoretical Force vs. Displacement Response of Experimental System with Four SMA Tube Springs 53
24	Transmissibility of SMA Spring-Mass System with Different Amplitude of Base Excitation for 1 kg Mass 55
25	Force-Displacement Response for an SMA Spring for the System with 1 kg Mass and 0.1 g Excitation Amplitude 56
26	Force-Displacement Response for an SMA Spring for the System with 1 kg Mass and 2.0 g Excitation Amplitude 57
27	System Response at Resonance for 1 kg Mass and 0.1 g Excitation 58
28	System Response at Resonance for 1 kg Mass and 3.0 g Excitation 59

FIGURE	Page
29	System Response for 1 <i>kg</i> Mass, 4 SMA Tube Springs, and 1.0 <i>g</i> Excitation Showing Reduction in Transmissibility (125 Hz) 61
30	Schematic of Shaker and SMA Spring-Mass Isolation System as Tested 64
31	Picture of SMA Spring-Mass Isolation Experiment Attached to Shaker Table 65
32	Picture of Shaker Assembly with Experiment Attached 66
33	Transmissibility for Case 1 69
34	Transmissibility for Case 2 70
35	Transmissibility for Case 3 71
36	Transmissibility for Case 4 72
37	Transmissibility for Case 5 73
38	Transmissibility for Case 6 75
39	Transmissibility for Case 7 76
40	Transmissibility for Case 8 77
41	Transmissibility for Cases 1 and 9, 1/4 <i>g</i> Loading 78
42	Transmissibility for Cases 1 and 9, 1/2 <i>g</i> Loading 79
43	Transmissibility for Cases 6 and 10, 1/4 <i>g</i> Loading 80
44	Transmissibility for Cases 6 and 10, 1/2 <i>g</i> Loading 81
45	Comparison of Numerical Simulation with Experimental Results for Cases 9 and 10 84
46	Comparison of Numerical Simulation with Experimental Results for Case 2 85
47	Comparison of Numerical Simulation with Experimental Results for Case 7 86

FIGURE		Page
48	Comparison of Numerical Simulation with Experimental Results for Case 8	87
49	Drawing for Experiment Base	101
50	Drawing for Experiment Side Support	102
51	Drawing for Experiment Excitation Plate	103
52	Drawing for Experiment Mass	104

LIST OF TABLES

TABLE		Page
I	Experimentally Determined Parameters for SMA Material Model . . .	30
II	Test Matrix for SMA Spring-Mass System	67

CHAPTER I

INTRODUCTION

Technology has advanced significantly in recent years, enabling significant increases in the performance of many types of devices while also allowing those devices to become smaller in size and mass. The advances in the design and manufacture of spacecraft is one area where the effect of advancing technology can be seen most clearly. Dumas notes that recent advances in technology have contributed significant improvements in performance while at the same time yielding reductions in size and mass, resulting in spacecraft that are more powerful and less expensive [1]. Casani also discusses the effect of advancing technology, noting the trend toward smaller spacecraft with very specific missions and clusters of small spacecraft whose combined abilities replace that of a much larger single craft [2]. Since one of the major costs of a spacecraft program is the cost involved with launch of the spacecraft into orbit [3], it is generally accepted that the smaller and lighter a spacecraft can be made, the less it will cost to put into orbit and the more cost efficient the spacecraft program will be. Along these lines, many of the newest technologies have been focused on efforts to develop methods to reduce the size and weight of spacecraft. However, a significant portion of the mass of a spacecraft is related to the supporting structure and not the actual components of the spacecraft. One of the primary reasons for the supporting structure in a spacecraft is that it aids in mitigating the harsh loading environment encountered during launch. Therefore, it would be possible to significantly reduce the complexity and mass of the spacecraft structure if the vibration loading experienced by the payload during launch could be reduced. In addition to reduction in the spacecraft mass, significant vibration

The journal model is *IEEE Transactions on Automatic Control*.

isolation would also result in a reduction in part count and an increase in both the reliability and service lifetime of a spacecraft [4]. Unwanted vibrations also affect the components of a spacecraft while on orbit and significant reductions in vibration loading for these components can result in increases in performance and the useful life of a spacecraft.

Since there is obvious and significant benefit to improved vibration isolation of spacecraft and their components, much effort has been directed at developing vibration isolation systems. There are two main types of vibration isolation devices currently under development for space systems, whole spacecraft isolation systems and component isolation systems. Whole spacecraft systems are designed to replace the fitting that mates the launch vehicle and the payload. In this manner, these devices can be designed so that they will inhibit transmission of vibration loads from the typically harsh environment of the launch vehicle to the sensitive payload. Component isolation systems are generally employed on orbit and are designed so that they will isolate a sensitive piece of equipment from the environment of the spacecraft. In some cases, they can be used to isolate a particularly noisy, but required, piece of equipment from the rest of the craft.

A. Recent Work in Spacecraft Vibration Isolation

Much of the work in the area of whole-spacecraft launch vibration isolation has centered around the use of conventional methods such as viscous dampers and the coupling of these conventional systems with active systems. The work of Edberg, et al, describes a series of isolation devices used to couple the payload to the launch vehicle, incorporating hydraulic dampers with either mechanical or pneumatic springs. These systems can be utilized either passively or actively (with feedback control) and

have demonstrated significant reduction in transmitted acceleration, with the active system reducing transmission to nearly zero [5, 6]. Wilke, et al, have developed a replacement payload attach fitting (PAF) with integrated passive hydraulic damping that is a one-for-one replacement for current PAF designs [7]. In another work by Wilke, et al, and in the work of Johnson, et al, the successful implementation of this hydraulic based passive vibration isolation for an entire spacecraft is discussed. This design, known as the SoftRide system, was successfully tested on two separate launches, providing a significant reduction in broadband structure-borne vibrations, especially in the targeted low frequency range [8, 9].

Work has also been done in the area of component isolation, where the main goal is to isolate the vibrating components of spacecraft while on orbit. Component isolation has centered mainly on active methods, or active systems coupled with passive systems for redundancy and better performance, and has been one of the first areas to see the introduction of smart structures and smart materials for use in vibration isolation of space systems. One example of an active system is the work of Yu, et al, which uses a high temperature super-conducting magnet as the soft link between the vibrating system and the isolated system [10]. Another example is the hybrid system presented by Cobb, et al, which uses active voice coil systems coupled with passive viscous damping [11]. In addition to vibration isolation, this system can also be utilized for precision pointing of spacecraft components such as communication antennas. A similar system utilizing piezoelectric actuators in place of voice coils systems was also investigated by Wada, et al [12]. Advances of these designs have been realized in the form of a piezoelectric based system for component isolation as described in the work of Anderson, et al [13]. This system is scheduled to fly on the PICOsat spacecraft and be tested to determine its on orbit performance. Of particular interest to this current work is the work of Yin and Regelbrugge [14], whose

investigation into the use of springs made from shape memory alloy for isolation of a spacecraft component. They have investigated passive isolation characteristics of the springs, both on orbit and during launch, and exploited the shape memory effect to maintain proper alignment of the protected equipment. A key result from their work is the ability to regain and maintain proper alignment of the protected equipment through exploitation of the shape memory effect of shape memory alloys.

B. Application of Shape Memory Alloys to Vibration Isolation

In addition to the work of Yiu and Regelbrugge mentioned above, the application of Shape Memory Alloys (SMA) to more standard isolation problems such as machinery and civil structures has been investigated and has shown much promise. Wolons, et al, have investigated the damping capacity of SMA wires through extensive experimentation and have found that SMA wires can have up to 20 times more damping capacity, per unit volume, compared to typical elastomers [15]. Fosdick and Ketema have performed a study of a single degree of freedom (SDOF) lumped mass oscillator with an SMA wire attached in parallel as a passive vibration damper and have shown that the hysteresis inherent in SMA to be most effective at low frequency [16]. Matsuzaki, et al, have also investigated the effect of introducing SMA elements into a dynamic system. Their study showed that the effect of introducing pre-strained SMA wires into a spring-mass system resulted in effective damping and suppression of disturbed motion [17]. Similar work by Turner has shown that the response of composite beams with embedded SMA wires subjected to random base excitation can be tailored by changing the temperature of the SMA wires [18]. The work of Graesser and Cozzarelli discussed the application of SMAs to the isolation of structures such as buildings, showing that SMAs may be suitable to damping the motions

induced by earthquakes [19]. The work of Wilde, et al, has built on the previous work of Graesser and Cozzarelli, applying SMA base isolation devices to highway bridges and achieving favorable results compared to the response of conventional base isolation devices [20]. A study of the use of SMAs in passive structural damping is also presented in the work of Thomson, et al, where three different quasi-static models of hysteresis were introduced and compared with experiments [21]. The work of Feng and Li has discussed the behavior of systems with solid SMA bars, showing a decrease in both the resonant frequency and resonant amplitude of a dynamic system when compared with other materials such as steel [22].

C. Objective of This Work

The objective of this research is to investigate the feasibility of utilizing the pseudoelastic shape memory alloy for the task of whole-spacecraft vibration isolation. It is believed that replacing current isolation devices with SMA based devices will result in lower mass, lower complexity and lower cost with equal or better performance. Vibration isolation is most often accomplished by joining two structures with a "soft link," a device or material with a low stiffness, with the goal of decreasing the force and motion transferred from one structure to the other [23]. However, a small stiffness will generally lead to large displacements when the loads involved are large, and this result is often unacceptable. Through the use of a device with decreasing stiffness, similar to an elastomer under buckling loads, it is possible to avoid large displacements while still achieving good isolation performance [24]. The basis for this work lies in the similarities between the force-displacement relation of the buckling elastomer and the force-displacement relation of the pseudoelastic SMA, as discussed below. While the goal of this proposal is to demonstrate the effectiveness

of the decreased stiffness during pseudoelastic transformation for reducing vibration transmissibility, it is felt that the hysteresis present in the loading behavior of SMA will also be beneficial in the frequency ranges of concern and will have a minimal negative impact on transmissibility at higher frequencies.

In order to determine the suitability of SMA for vibration isolation, accurate material level modelling of a system which includes structural members composed of SMA must be achieved. This modelling must be able to accurately predict the dynamic response of an SMA isolator and must incorporate a physically based material model for the behavior of shape memory alloys. Finally, correlation between this system model and actual experimental results must be achieved in order to validate the model. The remainder of this work will adhere to the following outline. First, an overview of shape memory alloys and the pseudoelastic effect will be presented. Following this, the development of a simplified material model for SMA pseudoelasticity which is suitable for dynamic analysis will be discussed. Next will be a discussion of the numerical solution of the dynamic system and the integration of the material model into this solution. After this section, the experiment designed to verify the numerical simulation will be discussed followed by results from a series of experiments conducted to determine the effect of pseudoelastic SMA on a dynamic system. After this will be a correlation between the model and experiments followed by a direction for future work, including ideas gained from the current work. Finally, conclusions drawn from this work will be presented.

CHAPTER II

SHAPE MEMORY ALLOY MATERIAL RESPONSE

In this chapter, an introduction to the mechanical behavior of SMA is presented along with a discussion of the significant work in the areas of SMA applications and modelling of SMA behavior. Finally, the similarities between the pseudoelastic behavior of SMAs and the behavior of a class of traditional vibration isolation devices are discussed.

A. Shape Memory Alloys

Shape memory alloys are a class of metals that have gained increasing recognition in previous years. These alloys exhibit a solid-to-solid phase transition characterized by a change in the crystallographic structure of the material. The driving force behind this phase change is a difference in the chemical free energy of the two phases, which in turn is dependent on both the temperature and the stress state of the material [25]. This phase change is referred to as martensitic phase transformation and is completely reversible and diffusionless in nature [26]. The martensitic phase transformation occurs between the parent phase, austenite, (A), and the martensitic phase, (M), of which there are several crystallographic variants [27]. During this transformation, the crystal structure of the material changes from a cubic arrangement (austenite) to a monoclinic arrangement (martensite) [28]. At the zero stress state, the martensitic transformation is characterized by the temperatures at which the transitions occurs. These temperatures are referred to as Martensite Start (M^{os}), Martensite Finish (M^{of}), Austenite Start (A^{os}), and Austenite Finish (A^{of}). This change in structure is the basis for pseudoelasticity, one-way shape memory effect (OWSME), and two-way shape memory effect (TWSME), which are the key behaviors of SMAs. Since

the focus of this work will be on pseudoelasticity, the reader is referred to the literature for further reading on OWSME and TWSME, which are commonly exploited in applications where the SMA is used as an actuator [29, 30, 31, 32, 33].

The behavior of pseudoelastic SMAs is more complex than many common materials as the stress-strain relationship is non-linear, hysteretic and exhibits large reversible strains due to the martensitic phase transformation. Pseudoelasticity is defined as being a martensitic phase transformation which is induced by a purely mechanical loading applied when the material is in the austenite phase (temperatures above A^{0s}) followed by a reverse transformation to austenite upon unloading. This loading causes the transformation of austenite into martensite with the variants realigned into a single crystallographic orientation. This reorientation, or detwinning, results in large strains that can be completely recovered upon unloading [34]. Figure 1a illustrates the relationship between stress, temperature, and phase in SMAs, and Figure 1b shows the pseudoelastic loading response that corresponds to the loading path denoted in Figure 1a.

B. Modelling of Vibration Isolation with SMA

The nature of the Pseudoelastic Effect, as discussed above and illustrated in Figure 1b, would indicate great potential in the application of SMAs to vibration isolation, especially in situations where the complexity of a device should be minimized. To date, a great deal of work has been accomplished in an effort to accurately model, on a constitutive level, the behavior of SMAs. The root behavior of SMAs, the crystallographic transformation that occurs as a result of changes in temperature and stress, is non-trivial to model constitutively and many different methods have been employed in an attempt to accurately model SMAs. Graesser and Cozzarelli, in their work mentioned

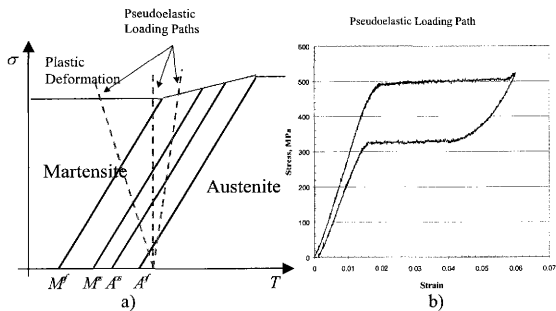


Fig. 1. a) Stress vs. Temperature Graph Indicating Start and Finish of Transformation Between Austenite and Martensite Phases. b) Pseudoelastic Loading Response of SMA

earlier [19], introduced a modified model for hysteretic behavior by Ozdemir [35] to model pseudoelastic behavior of SMAs, using ideas from viscoplasticity [36]. Feng and Li presented a modified plasticity model which was used to model the hysteretic response of the shape memory material [22]. Fosdick and Ketema have considered rate dependency by including “averaged” thermal effects based on the dynamics of single-crystal phase boundaries [37] in their work, also mentioned earlier [16]. Other work on constitutive modelling of SMAs includes phenomenological models by Lagoudas, et al [38], Lagoudas and Bo [39], Brinson [40], Liang and Rogers [41], Tanaka [42] and Sato and Tanaka [43], micromechanical models for polycrystalline SMAs by Patoor, et al [44] and Falk[45] and empirical models based on system identification (ID) by Preisach [46], Mayergoyz [47], Banks, et al [48, 49], Webb [50] and Webb, et al[51]. Although these models are fairly accurate, they are computationally intensive and/or hard to implement under dynamic loading conditions. Additionally, the nature of the Pseudoelastic Effect as it can be applied to vibration isolation through the utilization of SMA springs has not been addressed by the above publications.

Motivated by the need to model the dynamic response of a system with SMA components, it became necessary to develop a computationally efficient model for SMA pseudoelasticity which would capture the essence of pseudoelastic behavior and allow for a timely calculation of the system response. To realize the goal of designing and simulating a smart structure for vibration isolation using SMAs, it is necessary to have structural models that can (a) incorporate a physically based constitutive response of SMAs and (b) can be used for prediction of dynamic response of smart structures. Most of the models available in the literature do not serve this dual purpose well. In this work, the hysteresis and softening stiffness exhibited during pseudoelasticity is predicted through the use of a physically based material model for SMA pseudoelasticity. *It should be noted that at the structural assembly-level,*

the force-displacement relationship is more useful than the actual material state. Therefore, pseudoelastic force-displacement response has been modelled and will be explained in the following chapter. The model as presented here is equally applicable to the prediction of any non-linear, hysteretic system whether it be in terms of stress-strain, force-displacement, or any other terms suitable to the problem at hand.

C. Similarities Between Traditional Isolators and the Pseudoelastic Behavior of SMAs

When a shape memory alloy is loaded while in the austenitic phase, it initially behaves as if it were elastic in nature, similar to the initially stiff response of a traditional isolation device. This initial elastic response would support the static loads placed on the isolator. As the stress continues to increase, a point is reached where the material begins to transform into the martensite phase. This transformation is characterized by a decrease in the stiffness of the material and would correspond to the softening of a traditional isolator. This transformation region would also be the ideal operating region of the isolation since loading in this region would be attenuated due to the softer response of the device. If the load continues to increase, the entirety of the material is transformed into martensite. After this stress induced martensite (SIM) transformation is complete, the materials will again begin to deform elastically, with a stiffness greater than that present during the transformation but not necessarily equal to the initial stiffness. If the SMA is again compared to a traditional isolation device, this area of the pseudoelastic behavior would correspond to an increased stiffness designed to limit total deflection. If the loading is now reversed, it will unload elastically until it reaches a point at which the stress is low enough to permit the transformation back into the parent austenite phase. As the stress continues to decrease,

the material transforms completely back to its austenite phase and then continues to unload elastically until the zero stress point is reached. During this unloading process, it is possible for the material to recover all of the induced strain, returning to its undeformed, initial condition at zero stress. In addition to the change in material properties and large recoverable strain during pseudoclastic transformation, there is some hysteresis which is an indicator of energy dissipation during the austenite to martensite and martensite to austenite transformations. This energy dissipation is proportional to the degree of transformation completed during a loading cycle for both complete and incomplete, or partial, transformations. These partial transformations are also referred to as minor loop hysteresis cycles [52].

CHAPTER III

SIMPLIFIED SHAPE MEMORY ALLOY MATERIAL MODEL

In this chapter, a simplified material model for pseudoelastic SMAs is developed and implemented. This model is capable of accurately predicting the behavior of SMAs at temperatures above the austenite finish temperature (A^{of}), the temperature at which the reverse transformation from martensite to austenite is complete. Additionally, this model is displacement driven and is dependent on the loading history to correctly predict the forward and reverse transformation behavior and the minor loop behavior of SMAs. The basis of the model is the assumption that the relationship between force and displacement in an SMA at temperatures above A^{of} can be accurately represented by a series of linear segments whose form is determined by the extent of transformation experienced. The development of this model will be addressed in the following three sections. The first section will deal with the determination of material response in force-displacement space from the minimum amount of required physical data. The second section will deal with prediction of major loop response, and the third section will deal with prediction of minor loop behavior of SMAs.

A. Determination of Material Force-Displacement Response

To begin to adequately determine the response of SMA material, one must be able to predict at what loading conditions the transformation between the austenite and martensite phases will begin and end. Additionally, this information must be available at all temperatures in which this model is to be valid ($T > A^{of}$). The model presented in this paper is dependent upon only a few material parameters which can be gathered from relatively simple thermomechanical tests and a calorimetric analysis. From a typical pseudoelastic force-displacement test, shown in Figure 2, performed at

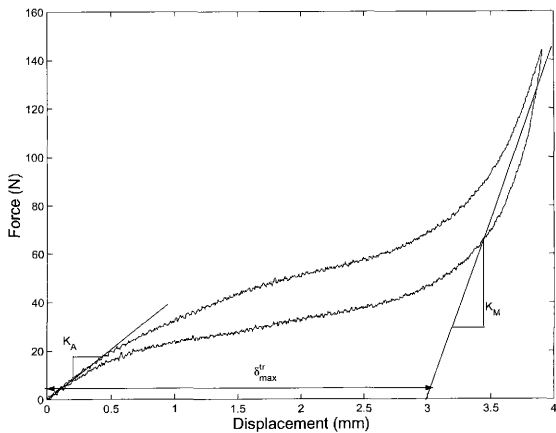


Fig. 2. Force vs. Displacement Response of Pseudoelastic SMA with K_M , K_A and δ_{max}^{tr} Labeled

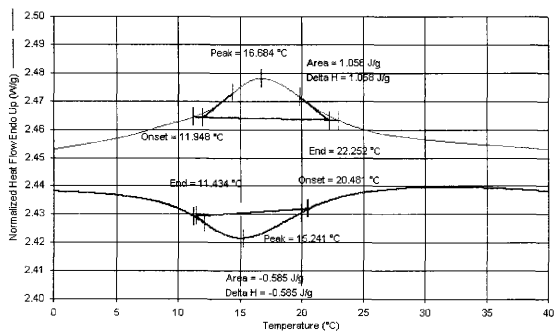


Fig. 3. Differential Scanning Calorimeter Results for SMA Material

a temperature greater than A^{of} , the stiffness of austenite (K_A) and martensite (K_M) as well as the maximum value of transformation displacement (δ_{max}^{tr}) can be obtained. Through the use of a Differential Scanning Calorimeter (DSC), the temperatures at which transformation occurs under zero stress can be determined. Figure 3 shows a DSC plot for the SMA material used in this work and is typical of most DSC results for SMA material. The information provided by the DSC measurement is the change in heat flow as a function of the change in temperature. Since the martensitic phase transformation is endothermic or exothermic depending on direction, the temperatures at which the transformations start and end can be estimated from the results of the DSC test. The results from the DSC data can be coupled with the results from the pseudoelastic tests to provide all the necessary material information for the simplified model.

For representation of force-displacement pseudoelasticity of an SMA component, a force-temperature phase diagram describing the relationship between force, displacement and phase can be constructed by one DSC measurement and one pseudoelastic response test, as shown in Figure 4. The assumption is made that the lines marking the transformation boundaries are parallel, which strictly speaking is not necessarily correct but for the purpose of this model does allow for a simplified representation of the pseudoelastic response. In this case, the zero stress transformation temperatures and the slope of the transformation boundaries are chosen based on the pseudoelastic response and the DSC tests, but modified slightly so that the pseudoelastic force-displacement relationship is preserved for the component. Another simplification is in the selection of the transition points between elastic loading and transformation. Due to the non-uniform stress state and polycrystalline nature of SMA components, some areas of the material will begin to transform before others, resulting in the smooth transitions seen in Figure 2. However, the simplified model presented here

requires specific transition points (points 1-4 in Figures 4 and 5) at which to begin and end the forward and reverse transformation. Therefore, points are chosen so that the pseudoelastic force displacement relationship is preserved. Once the simplifications are made and the appropriate constants are chosen, the simplified model utilizes the force-temperature phase diagram (Figure 4) to create a piecewise linear representation of the pseudoelastic response of the SMA shown in Figure 2. From the force-temperature diagram and given that the temperature of the SMA is known and constant, it is possible to calculate the forces at which the forward and reverse transformations begin and end from Equation 3.1 where f^t is the force, C is the slope of the transformation boundary in the force-temperature plane, T is the temperature, and T^t is the zero-stress transition temperature determined from the DSC results for the respective transition.

$$f^t = C(T - T^t) \quad (3.1)$$

Additionally, the constitutive relation for SMA can be modified to yield Equation 3.2, where K_p is the respective stiffness of either austenite, martensite or a mixture of the two phases, δ is the total applied displacement and δ^{tr} is the transformation displacement of the SMA. Transformation displacement for a force-displacement model is similar to the transformation strain for a stress-strain model.

$$f = K_p(\delta - \delta^{tr}) \quad (3.2)$$

Given that the material state is assumed to be known at the beginning and end of transformation for both forward and reverse transformation, one can calculate the displacement at which transformation will occur. Using this data, one can construct the following force-displacement diagram as shown in Figure 5 using only the material parameters mentioned above. For this simplified model of pseudoelastic loading, the

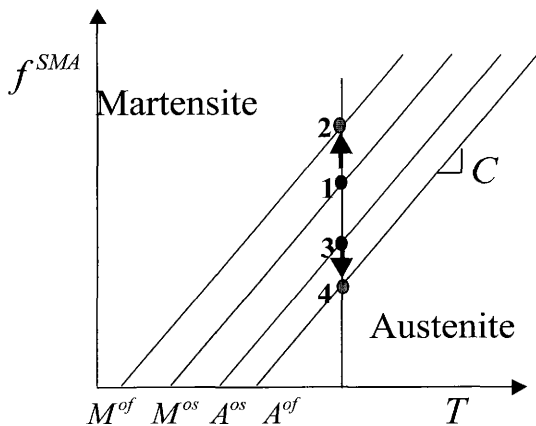


Fig. 4. SMA Force-Temperature-Phase Diagram with Pseudoelastic Loading Path

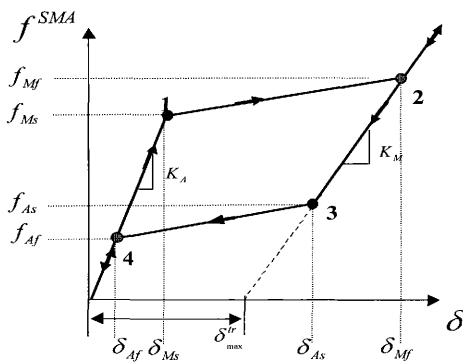


Fig. 5. Simplified Pseudoclastic Force vs. Displacement Response of SMA for Major Loop Loading

transitions delineating the beginning and end of forward and reverse transformation are dependent only upon the ambient temperature and the material parameters, including the zero load transition temperatures, the transformation displacement and the stiffness of the two phases. For the beginning of the austenite to martensite, or forward, transformation (point 1 on Figure 5), the corresponding force and displacement are calculated from Equations 3.3 and 3.4.

$$f_{Ms} = C(T - M^{os}) \quad (3.3)$$

$$\delta_{Ms} = \frac{C(T - M^{os})}{K_A} \quad (3.4)$$

For the end of the forward transformation (point 2), the corresponding force and displacement are calculated from Equations 3.5 and 3.6.

$$f_{Mf} = C(T - M^{of}) \quad (3.5)$$

$$\delta_{Mf} = \frac{C(T - M^{of})}{K_M} \quad (3.6)$$

For the beginning of the martensite to austenite, or reverse, transformation (point 3), the corresponding force and displacement are calculated from Equations 3.7 and 3.8.

$$f_{As} = C(T - A^{os}) \quad (3.7)$$

$$\delta_{As} = \frac{C(T - A^{os})}{K_M} \quad (3.8)$$

For the end of the reverse transformation (point 4), the corresponding force and displacement are calculated from Equations 3.9 and 3.10.

$$f_{Af} = C(T - A^{of}) \quad (3.9)$$

$$\delta_{Af} = \frac{C(T - A^{of})}{K_A} \quad (3.10)$$

Assuming piecewise linear response and combining all of this information together

will result in completely determining the force-displacement response of an SMA for a full loading induced transformation cycle, as shown schematically in Figure 5.

B. Major Loop Loading

To correctly predict the force-displacement response of an SMA, the loading path for full transformation, or the major loop, must be modelled. For the simplified material model, this is accomplished by assuming that both the transformation displacement, δ^{tr} , and the force, f , vary linearly during transformation and that the force corresponds to displacement in a linear manner when transformation is not occurring. As a result, the SMA material can be modelled as a series of straight lines in force-displacement space, where the intersection of these lines correspond to the transition between elastic loading and transformation for forward and reverse transformation. This can be illustrated schematically, as shown in Figure 5. For elastic loading in the austenite region ($4 \rightarrow 1$) prior to the beginning of forward transformation, the transformation displacement remains zero and the force is directly related to the displacement. This is explicitly stated in Equations 3.11 and 3.12.

$$\delta^{tr} = 0 \quad (3.11)$$

$$f^{SMA} = K_A \delta \quad (3.12)$$

For forward transformation, the region between points 1 and 2, the transformation displacement varies linearly between zero and the maximum value of transformation displacement, δ_{max}^{tr} . Additionally, the force level also varies linearly between the force levels corresponding to the beginning and end of transformation. Mathematically this

is shown below in Equations 3.13 and 3.14.

$$\delta^{tr} = \delta_{max}^{tr} \left(\frac{\delta - \delta_{Ms}}{\delta_{Mf} - \delta_{Ms}} \right) \quad (3.13)$$

$$f^{SMA} = f_{Ms} + \frac{\delta^{tr}}{\delta_{max}^{tr}} (f_{Mf} - f_{Ms}) \quad (3.14)$$

At strain levels above the martensite finish level, the region after point 2, the force again relates linearly to the displacement and the transformation displacement remains at a constant value equal to δ_{max}^{tr} . This relation remains true even after the onset of unloading until the beginning of reverse transformation begins (point 3) as shown in Equations 3.15 and 3.16.

$$\delta^{tr} = \delta_{max}^{tr} \quad (3.15)$$

$$f^{SMA} = f_{Mf} + K_M(\delta - \delta_{Mf}) \quad (3.16)$$

After the beginning of reverse transformation (point 3) and before the transformation to austenite completes (point 4), the transformation displacement again varies linearly, this time between δ_{max}^{tr} and zero. Likewise, the force varies linearly between the value at the start of reverse transformation and the value at the end of transformation. This is shown in Equations 3.17 and 3.18.

$$\delta^{tr} = \delta_{max}^{tr} - \delta_{max}^{tr} \left(\frac{\delta_{As} - \delta}{\delta_{As} - \delta_{Af}} \right) \quad (3.17)$$

$$f^{SMA} = f_{Af} + \frac{\delta^{tr}}{\delta_{max}^{tr}} (f_{As} - f_{Af}) \quad (3.18)$$

At the conclusion of reverse transformation, the transformation strain is again zero and the force again varies linearly with the displacement, as show in Equations 3.11 and 3.12.

C. Minor Loop Loading

To accurately model SMAs for a particular application, it becomes necessary to model the minor loop loading cycles. Minor loop loading cycles are those loading cycles that do not result in complete transformation from austenite to martensite and back to austenite. From inspection of Figure 6, which illustrates a minor loop displacement loading path, it becomes clear that in order to model this behavior, some modifications must be made to the equations above to account for this incomplete transformation. As a result of the simplicity of this model, the modifications are easy to implement. The first issue that must be dealt with is the dependence of the current material behavior on the history of loading of the material. This can be accomplished by storing the maximum and minimum values of force, displacement and transformation displacement for the previous loading cycle. The second issue to be dealt with is the modification of the points in force-displacement space that initiate the beginning of forward and reverse transformation. The third issue relates to the *stiffness* of the material. As the material transforms between austenite and martensite, the stiffness of the material changes between the stiffness of each phase. The stiffness at any given point during transformation is calculated using a rule of mixtures on the compliance of the individual phases.

Figure 7 depicts a minor loop case. When loading from zero force in the austenite phase, the equations are the same as for the initial elastic loading and the forward transformation. However, for a minor loop loading path, the loading is reversed prior to completion of forward transformation at point R . At this point, the maximum values of force, displacement, and transformation displacement are recorded, as they will be used in subsequent calculations. As unloading begins from point R to 3, initially there is no transformation so that the unloading occurs elastically, but at a

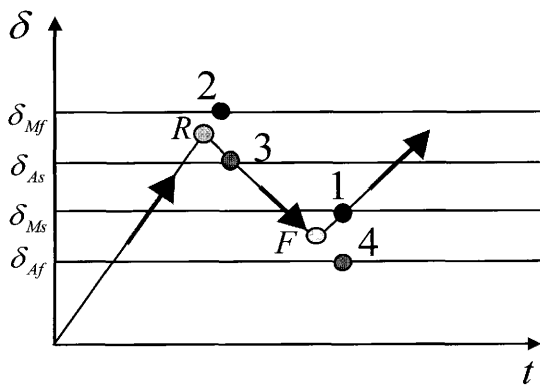


Fig. 6. Representative Displacement Path for Minor Loop Loading

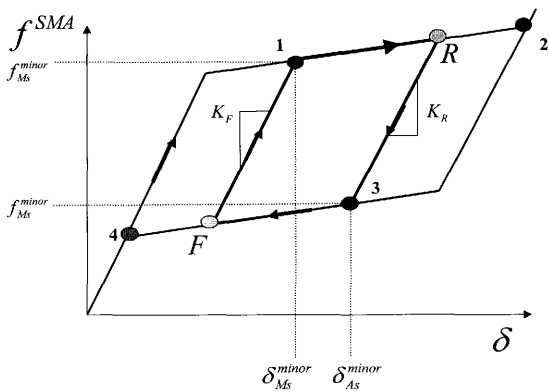


Fig. 7. Simplified Pseudoelastic Force vs. Displacement Response of SMA for Minor Loop Loading

stiffness that is neither the austenite stiffness nor martensite stiffness. Unloading occurs elastically from the maximum transformation point and the slope is determined by the maximum degree of transformation obtained. For this portion of the force-displacement relation, the unloading stiffness, K_R , and the force are calculated as shown in Equations 3.19 and 3.20 where δ_R^{tr} , f_R , and δ_R are the values of transformation displacement, force and displacement recorded when the loading path changed directions.

$$K_R = \frac{K_M K_A}{\frac{\delta_R^{tr}}{\delta_{max}^{tr}}(K_A - K_M) + K_M} \quad (3.19)$$

$$f^{SMA} = f_R + K_R(\delta - \delta_R) \quad (3.20)$$

The transformation strain remains constant for this section of the loading path, since the unloading is elastic and no transformation occurs. As the material continues to unload, the path it is following will eventually intersect the line for major loop reverse transformation (point 3), where reverse transformation begins for minor loop loading paths. Due to the incomplete forward transformation, this point is different from the (f_{As}, δ_{As}) pair denoting point 3 in Figure 5 and is defined by Equations 3.21 and 3.22.

$$\delta_{As}^{minor} = \delta_{As} + \frac{\delta_R^{tr}}{\delta_{max}^{tr}}(\delta_{As} - \delta_{Af}) \quad (3.21)$$

$$f_{As}^{minor} = f_{As} + \frac{\delta_R^{tr}}{\delta_{max}^{tr}}(f_{As} - f_{Af}) \quad (3.22)$$

As this point is reached, reverse transformation begins and the following equations will determine the values of transformation displacement and force from point 3 onwards.

$$\delta^{tr} = \delta_{max}^{tr} - \delta_{max}^{tr} \frac{\delta_{As}^{minor} - \delta}{\delta_{As}^{minor} - \delta_{Af}} \quad (3.23)$$

$$f^{SMA} = f_{Af} + \frac{\delta^{tr}}{\delta_{max}^{tr}}(f_{As}^{minor} - f_{Af}) \quad (3.24)$$

As the material continues to unload, the force will decrease and the transformation

displacement will go to zero as the material approaches point 4 where reverse transformation ceases. At this point, the material will be entirely in austenite again and will unload elastically to zero load. Now, if the material does not unload entirely into austenite but again changes the loading direction and begins to load again, the force, displacement, and transformation displacement at this point must again be recorded. This point is shown as point F in Figures 6 and 7. As the material begins to load from point F to 1, it again loads elastically at a stiffness determined by the minimum degree to which transformation had progressed. The stiffness and force level are given in Equations 3.25 and 3.26 where δ_F^{tr} , f_F , and δ_F are the values of transformation displacement, force and displacement recorded when the loading path changed directions.

$$K_F = \frac{K_M K_A}{\frac{\delta_F^{tr}}{\delta_{max}^{tr}}(K_A - K_M) + K_M} \quad (3.25)$$

$$f^{SMA} = f_F + K_R(\delta - \delta_F) \quad (3.26)$$

From this point, the material loads elastically until this loading path intersects with the forward transformation path for major loop loading (point 1). This point is calculated in a similar manner to that used in the calculation of the beginning of reverse transformation and is again based on the intersection of the major loop loading path and the minor loop loading path. The formulas defining this point are given in Equations 3.27 and 3.28.

$$\delta_{Ms}^{minor} = \delta_{Ms} + \frac{\delta_F^{tr}}{\delta_{max}^{tr}}(\delta_{Mf} - \delta_{Ms}) \quad (3.27)$$

$$f_{Ms}^{minor} = f_{Ms} + \frac{\delta_F^{tr}}{\delta_{max}^{tr}}(f_{Mf} - f_{Ms}) \quad (3.28)$$

From this point, force and transformation displacement for forward transformation are calculated in a manner similar to that used in the calculation of force and trans-

formation displacement for the reverse transformation. The equations are as follows:

$$\delta^{tr} = \delta_{max}^{tr} \frac{\delta - \delta_{Ms}^{minor}}{\delta_{Mf} - \delta_{Ms}^{minor}} \quad (3.29)$$

$$f^{SMA} = f_{Ms}^{minor} + \frac{\delta^{tr}}{\delta_{max}^{tr}} (f_{Mf} - f_{Ms}^{minor}) \quad (3.30)$$

The continuation of loading along this path will result in complete transformation to martensite as described in the major loop section. A change in loading direction prior to complete transformation will result in additional minor loops and the preceding equations are applicable.

D. Characterization of SMA Tubular Springs

In order to calibrate the simplified pseudoelasticity model presented here, data from a thermal scan of the SMA material and a pseudoelastic compression test of the tubular springs are required. The thermal scan was performed using a Perkin Elmer Pyris 1 Differential Scanning Calorimeter (DSC) and measures the temperatures at the beginning and end of forward and reverse phase transformation at zero load. The thermal scan data is presented in Figure 3. The mechanical test was performed on an MTS servo-hydraulic load frame with a TestStar II controller under displacement control, where the tube was loaded transverse to the longitudinal axis in increments up to approximately seventy percent reduction in diameter. Various loading rates were used ranging from 0.016 mm/s to 0.3 mm/s . These loading rates all yielded the same results, and no change in the temperature of the SMA material was noted, implying that the isothermal assumption of the simplified material model is an acceptable simplification for this case. Experimentally determined force-deflection behavior for the SMA pseudoelastic spring, along with the output for the spring model as calibrated for use in this work, is shown in Figure 8. In order to calibrate the model for the

SMA spring, it was necessary to implement the assumptions listed earlier concerning the beginning and end of transformation for both force displacement space and force temperature space. From the experimental data, it is evident that the slope of the transformation regions in force temperature space are not parallel. However for this work a median value of $6 N/^{\circ}C$ was chosen. Additionally, it is obvious that for this component there is not a single point marking the beginning or ending of any of the transformation regions so it was again necessary to choose a point that would allow for the best representation of the force displacement response. As a result of these assumptions, it was then necessary to modify the zero load transformation temperatures slightly from the values measured during the DSC tests. The values used to calibrate the model are shown in Table I and, as shown in Figure 8, they do provide a good representation of the experimental data.

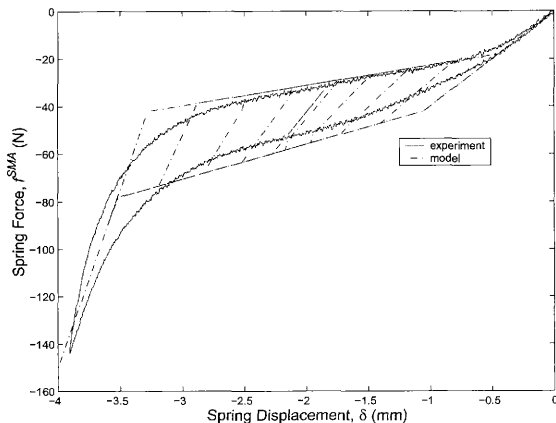


Fig. 8. Force vs. Displacement Response of SMA Tube Spring with Response from Simplified Pseudoelastic Model Showing Major and Minor Loop Response as Calibrated for This Work

Table I. Experimentally Determined Parameters for SMA Material Model

M^{of} = 12 °C	K_A = 40 KN/m
M^{os} = 18 °C	K_M = 150 KN/m
A^{os} = 18 °C	δ_{max}^{tr} = 3 mm
A^{of} = 22 °C	C = 6 N/m
T = 25 °C	

CHAPTER IV

DEVELOPMENT OF SMA VIBRATION EXPERIMENT

While the work presented thus far can be applied to any system whose spring force can be generalized as nonlinear and hysteretic, the experimental work conducted has focused specifically on the investigation into the use of thin-walled SMA tubes, compressed transverse to the longitudinal axis, as vibration isolators. The decision to utilize SMA tubes for this investigation was based on their ability to recover completely after nearly seventy percent compression at relatively low force levels, their ease of incorporation into a vibration test design, and their ready availability. The tubes were acquired from Shape Memory Applications, Inc. and were manufactured from binary NiTi with an outer diameter of approximately 6mm and an inside diameter of approximately 5.95mm. The tubes were supplied in approximately one-half meter length and subsequently cut to 10mm lengths.

An experiment was created for the express purpose of determining the effect of pseudoelastic SMAs used in a dynamic system to replace the spring in a traditional spring-mass system. SMA thin walled tubes, used as compression springs, were used to connect the mass to a base subjected to a given excitation level. Since the SMA tubes would only function in compression, the experiment was designed such that the SMAs could be preloaded so that they would always operate in compression. The amount of compression was chosen such that the SMA would operate in the hysteretic region of the pseudoelastic response. A schematic of the SMA spring-mass system as designed is shown in Figure 9. The system is excited by motion of the base plate, whose motion is denoted by y . The experiment was designed so that the SMA springs operated in pairs to provide resistance to both tension and compression for the system as a whole, while always being compressed on an individual basis

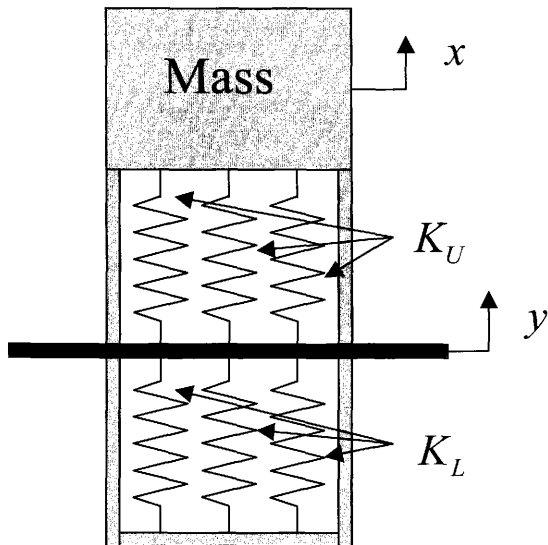


Fig. 9. Schematic of SMA Spring-Mass Isolation System as Designed

to some extent. This is shown in Figure 10. In Figure 10a, the SMA spring-mass system is shown in the unloaded configuration. In this configuration, the springs above and below the plate, labelled y , would be in compression. In Figure 10b, the system is in compression, as denoted by the motion of the plate and the notation $y > y_0$. In this configuration, the springs above and below the plate are still in compression. However, the springs above the plate are compressed more with respect to the unloaded configuration and the springs below the plate are compressed less with respect to the unloaded configuration. In Figure 10c, the system is in tension, again denoted by the motion of the plate and the notation $y < y_0$. The springs above and below the plate are again in compression. However, now the springs below the plate are compressed more with respect to the unloaded configuration and the springs above the plate are compressed less with respect to the unloaded configuration. The initial compression of the springs is referred to as the pre-compression and is given as a percentage of the initial undeformed length of the springs. This pre-compression will dictate the point about which the springs will operate in the transition region of the pseudoelastic response. Variations in the amount of pre-compression will affect both the stiffness of the system and the energy absorbed by the hysteresis of the SMAs. Mechanical drawings for this experiment are included in Appendix A. An assembly scene created from the mechanical drawings of the experiment is shown in Figure 11. Figure 12 shows a detail drawing of how the SMA tube springs are mounted in the experiment. Due to the pre-compression, the small depression will prevent the tube from moving around during testing, while the radius of the depression is chosen so that it will maintain a single point of contact boundary condition at all but the most extreme deformations.

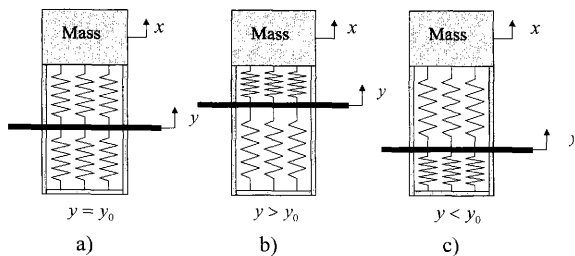


Fig. 10. Various Schematics of SMA Spring-Mass Isolation System

- a) Schematic of SMA Spring-Mass Isolation System in the Unloaded State
- b) Schematic of SMA Spring-Mass Isolation System in Compression
- c) Schematic of SMA Spring-Mass Isolation System in Tension

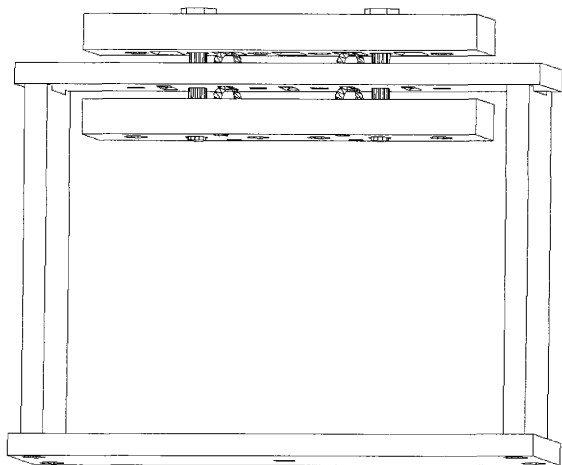


Fig. 11. Assembly of Vibration Isolation Experiment

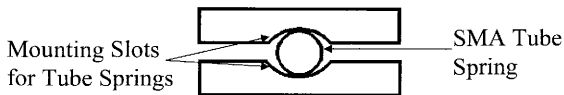


Fig. 12. Detail of SMA Tube Spring Mounting

CHAPTER V

DEVELOPMENT OF NUMERICAL SIMULATION OF A VIBRATING SYSTEM
WITH SMA SPRINGS

A computationally efficient simplified material model for pseudoelasticity in SMAs was developed in the previous chapter. That model is now used to solve the coupled structural response of a dynamic system involving SMAs. The simplified material model is integrated into the numerical solution of a single degree of freedom spring mass system where the restoring force of the springs is provided by the pseudoelastic response of SMA components.

A. Analysis of the Single Degree of Freedom Dynamic System

A schematic of the SMA spring-mass system along with a free-body diagram of the mass being isolated is shown in Figure 13. Note that the system described in Figure 13 is equivalent to the one described previously and shown in Figure 9. The system is excited by the motion of the supporting structure, denoted by y . From the free body diagram in Figure 13b, the equation of motion for the system can be determined as shown in Equation 5.1, where m is the mass to be isolated, \ddot{x} is the acceleration of the isolated mass, and N_u and N_l refer to the number of springs on the upper or lower sides of the mass, respectively. The forces exerted by the SMA springs, f_u^{SMA} and f_l^{SMA} , are determined by the displacement of the springs, δ_u and δ_l , and the displacement history of the springs as discussed previously. These displacements are functions of x and y as shown in Equation 5.2. It should be noted that due to the non-linear nature of the force-displacement relationship for these springs, both the

upper springs and lower springs must be modelled independently of each other.

$$m\ddot{x} = N_u f_u^{SMA}[\delta_u(t)] - N_l f_l^{SMA}[\delta_l(t)] \quad (5.1)$$

$$\delta_l = -\delta_u = x - y \quad (5.2)$$

Excitation of the system is introduced through sinusoidal motion of the base of the device whose magnitude is determined by the desired loading to be placed on the structure. Loading magnitude, a , is specified as a fraction of the acceleration due to gravity, g . Loading frequency is specified in cycles per second, denoted as f . The acceleration due to gravity is taken as 9.81 m/s^2 . The magnitude of displacement necessary to achieve a required acceleration at a given frequency is determined by the relationship shown in Equation 5.3, given that the motion is sinusoidal and periodic.

$$y = \frac{ag}{(2\pi f)^2} \quad (5.3)$$

The transmissibility, TR , of the system, a measure of the force or motion transmitted through the system, is defined as the magnitude of the output motion divided by the magnitude of the input motion. This is shown mathematically in Equation 5.4. For a linear system, the transmissibility can be derived analytically as shown in Equation 5.5.

$$TR = \frac{|x|}{|y|} \quad (5.4)$$

$$TR = \frac{1}{1 - (\frac{f}{f_n})^2} \quad (5.5)$$

With both the dynamic system and the response of the SMA springs defined, it is now possible to model the system as depicted in Figure 13 and described by Equation 5.1. The following section describes the numerical implementation used to solve Equation 5.1.

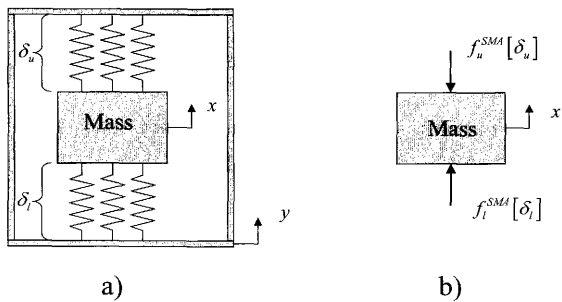


Fig. 13. a) Schematic of SMA Spring-Mass Isolation System. b) Free Body Diagram of SMA Spring-Mass Isolation System

B. Numerical Implementation of Solution to SDOF System with SMA Components

The simulation of the dynamic system was developed in the MATLAB environment [53]. After successful implementation, the simulation was converted to C++ in order to address deficiencies in the execution efficiency. Time history response of the system was calculated using a Newmark integration method with time step and weighting factors chosen to ensure stability of both the integration and the material model describing the spring behavior [54, 55]. The time integration is accomplished by a constant-average acceleration variant of the Newmark method. For $t = t_n$ the Newmark method is defined by Equations 5.6 and 5.7 for which the constant-average acceleration method (trapezoidal rule) is obtained if $\alpha = \frac{1}{2}$ and $\gamma = \frac{1}{2}$.

$$x_{n+1} = x_n + \Delta t \dot{x}_n + \frac{1}{2}(\Delta t)^2((1 - \gamma)\ddot{x}_n + \gamma\ddot{x}_{n+1}) \quad (5.6)$$

$$\dot{x}_{n+1} = \dot{x}_n + \Delta t((1 - \alpha)\ddot{x}_n + \alpha\ddot{x}_{n+1}) \quad (5.7)$$

The selection of this second order implicit method was governed by the highly non-linear nature of the differential equation describing the system. For a linear system, this scheme conserves the total energy of the system, allowing the high-frequency response to be simulated without any numerical damping and is unconditionally stable. Therefore, this same scheme is used to solve the non-linear, hysteretic SMA spring-mass system based on the understanding that unconditional stability holds for certain non-linear systems. However, no proof of stability for this type of non-linear systems is available. For a detailed discussion on time-integration schemes, the reader is referred to the work of Hughes [56]. Final implementation of this code allows for calculation of both time history of the mass motion at a given frequency and amplitude and the transmissibility of the system when subjected to a given amplitude excitation over a range of frequencies. The calculation of transmissibility is performed by analyzing the results of a series of time history calculations over the

frequency range of interest with transmissibility at each excitation frequency being calculated according to Equation 5.4.

A flowchart depicting the calculation of time history for a given frequency is presented in Figure 14. As shown, the parameters governing the system such as mass, number of springs, excitation level and frequency, and initial conditions along with the material parameters for the simplified material model are input first. Next the system is initialized according to the initial conditions, and the calculation of time history is begun. For a given timestep, the position of the mass is first estimated from the previous position. With this estimation and the position of the base, which is given, the displacement of the springs can be calculated. The force exerted by the spring and the transformation displacement are then calculated using the simplified SMA pseudoelastic model based on the spring displacement and loading history of the springs. Loading history is always considered from the last valid timestep, not the last position estimate at the current timestep. In this manner, it is assured that the material model always produces an accurate prediction of the force produced by the SMAs, which in turn is necessary for accurate prediction of position at the current timestep. After force and transformation displacement are calculated, a new estimate of the position of the mass is calculated and compared to the previous estimation. If the two estimations are within the given tolerance, the estimation is considered correct and the calculations proceed for the next timestep. It should be noted that the transformation displacement is not used in the calculation of position, however it is used to monitor the degree of transformation completed and, as such, is required for accurate calculation of the force exerted by the SMA. After calculation of the final timestep, the simulation routine ends and the time history data is available for analysis to determine transmissibility, motion of the mass or force-displacement response of the SMA springs. As mentioned earlier, this numerical solution was prototyped in

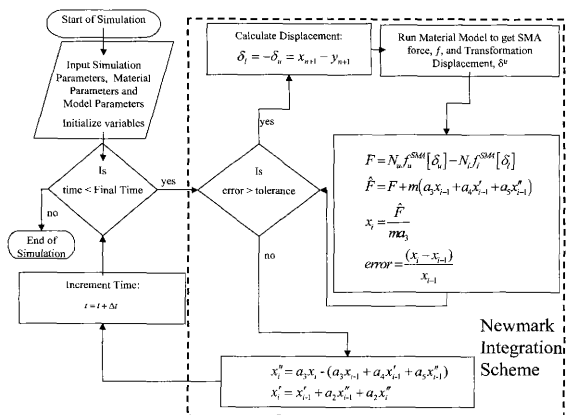


Fig. 14. Flowchart of Algorithm Used to Calculate the Time History of the Dynamic System

MATLAB and then converted to C++. Appendix B contains the source code for the MATLAB implementation, which has been included instead of the C++ code since it is more platform independent and does not require the custom graphics libraries used in the C++ code. Figure 15 shows several screen captures of the C++ code during operation.

C. Validation of Numerical Integration

Figure 16 shows the displacement response of a linear spring-mass system identical to that shown in Equation 5.1, except that the spring force has a linear relationship to displacement. This is accomplished by preventing the model for pseudoelastic behavior to begin phase transformation so that the system behaves as if it were linear elastic with a stiffness equal to that of the austenite phase. This system was solved using the Newmark integration method, as shown above, and these results are shown along with the analytical solution for this linearized system. Comparison is shown in Figure 16 for a system having $m = 1kg$, $K_A = 40N/m$, $N_l = N_u = 1$, $a = 1$, and a forcing frequency equal to one and a half times the natural frequency, which for this system is 45 Hz. Figure 17 shows the transmissibility of this linear spring-mass system for a range of frequencies, calculated using the above mentioned Newmark method, as well as the analytical expression for transmissibility (see Equation 5.5). From both Figure 16 and Figure 17, it can be seen that the Newmark method agrees well with the analytical solutions for the given linear system.

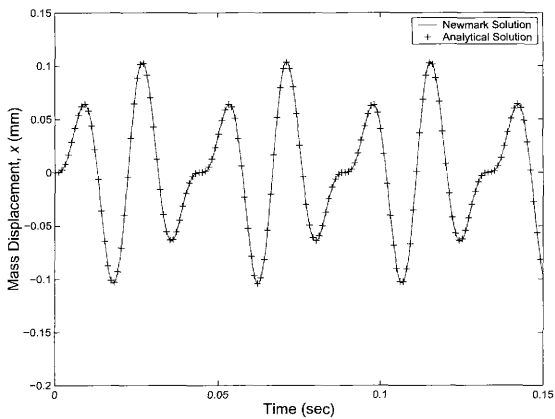


Fig. 16. Response of Linearized Spring-Mass System Calculated Using Newmark Method and Analytical Solution

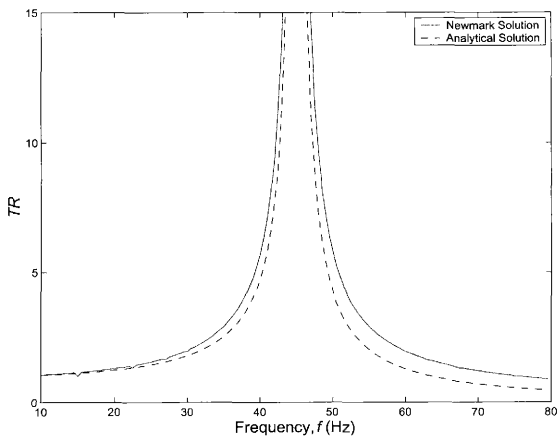


Fig. 17. Transmissibility for a Linear Spring-Mass System, Using Newmark Method and Analytical Solution

D. Investigation into the System Response of the Prototype SMA Based Isolation Device

After development of the experiment and of the numerical simulation, an investigation was started to determine the system response of the experimental system. An initial numerical investigation was completed to determine the effect of the SMA springs operating in opposition to each other. The behavior predicted was then verified by quasi-static mechanical testing of the prototype device.

1. Numerical Prediction of System Response

In order to investigate the system response, a simple simulation based on the previously discussed simplified model for pseudoelasticity was performed. In this simulation, two springs were modelled as they would operate in the prototype as shown in Figure 10. Figure 18 shows the response of the individual springs after being pre-compressed to 2 mm and subjected to a $\pm 1\text{ mm}$ displacement. As shown in the figure, the upper spring first begins to unload as the lower spring begins to load, just as the system was designed. As the direction of the displacement changes, the upper spring begins to load as the lower spring unloads. Since the material is non-linear and hysteretic, the changes in the force are not equal for equal changes in displacement. This results in the hysteretic system response shown in Figure 18.

Further study was undertaken to determine the effect of changes in the pre-compression and amplitude of motion on the system response. These results are presented in Figures 19 and 20. As shown in Figure 19, changing the pre-compression level can have dramatic changes in the system response and it appears that values of between 1.5 mm and 2 mm produce the best system response for this level of displacement amplitude. It should be noted that the irregularities in the response

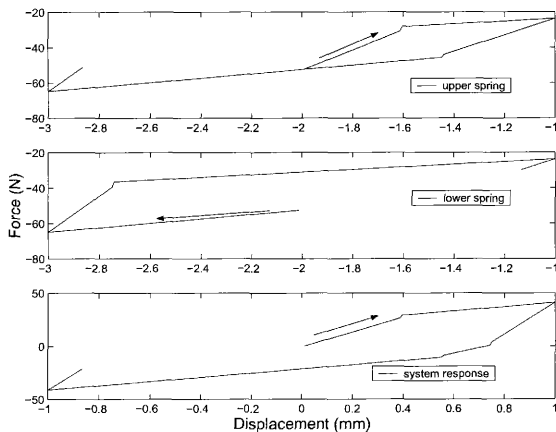


Fig. 18. Individual Tube Spring and System Response for Pre-Compression of 30% of Tube Diameter

seen for pre-compression levels of 1 mm and 2.5 mm are due to one of the springs entering an elastic region and thus undergoing a large change in the stiffness, resulting in large changes in the force for small changes in the displacement. Figure 20 shows the effect of changing the amplitude of displacement for a constant pre-compression of -2 mm. These figures show that as the displacements increase the hysteresis of the system response increases, resulting in more energy being absorbed by the system.

2. Experimental Investigation of System Response

Following this modelling effort, several experiments were performed to determine if the actual system response would be similar to the system response predicted by the numerical simulation. Figure 21 shows the force-displacement response of the experimental system with four SMA spring tubes tested quasi-statically, and Figure 22 shows the response for the system with six spring tubes. Both tests were performed on the MTS equipment described earlier. Figure 23 presents a comparison of the experimental data presented in Figure 21 and data collected from the numerical simulation. As shown, these two data sets are in close agreement with each other. However, it was necessary to increase the pre-compression input into the simulation by 50% over the value measured during the experimentation. After careful evaluation, it has been determined that the most likely cause of this discrepancy is due to inaccurate measurement of the pre-compression of the experiment or as a result of the simplified model not being capable to represent the gradual onset of transformation.

E. Simulation Results Based on Proposed Experiments

Based on the experimental design discussed in the previous chapter, an investigation into the anticipated system performance was conducted as detailed below. The pur-

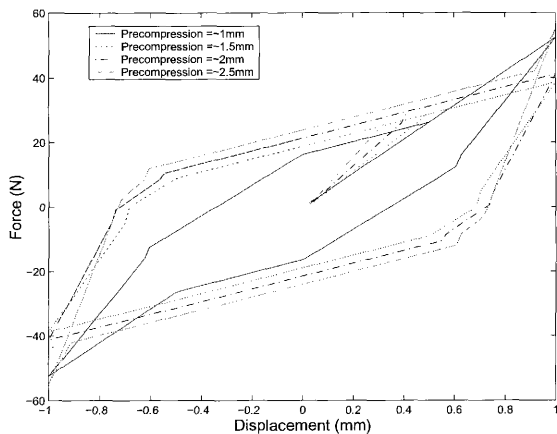


Fig. 19. System Response for Various Levels of Pre-Compression at a Displacement Amplitude of ± 1 mm

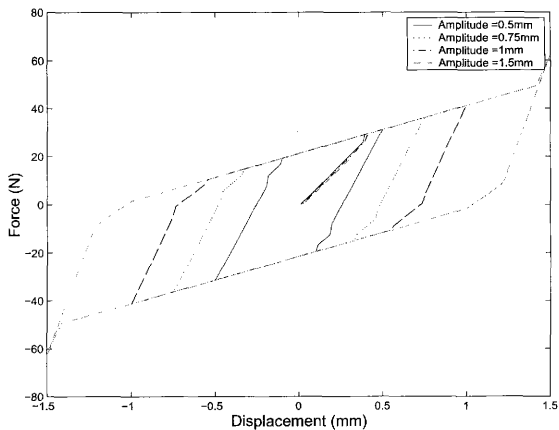


Fig. 20. System Response for Various Amplitudes of Displacement at a Pre-compression Level of -2 mm

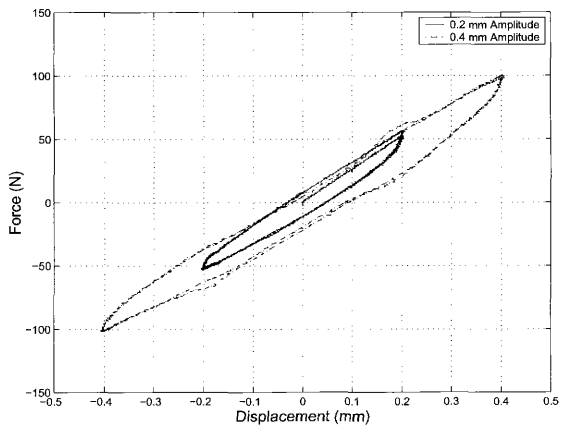


Fig. 21. Quasi-Static Evaluation of the Force vs. Displacement Response of the Experimental System with Four SMA Tube Springs $\left(\begin{array}{c} \circ \circ \\ \circ \circ \end{array}\right)$

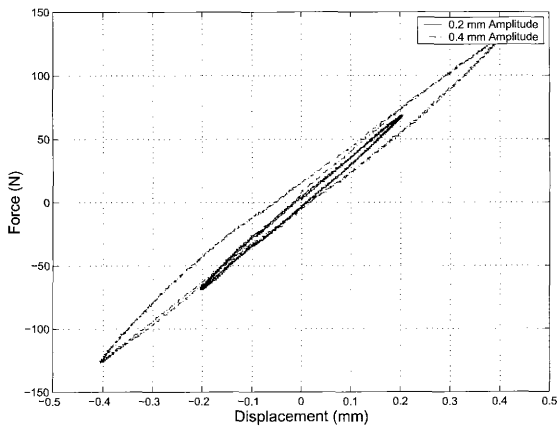


Fig. 22. Quasi-Static Evaluation of the Force vs. Displacement Response of the Experimental System with Six Tube Springs $\left(\begin{array}{c} \circ \circ \circ \\ \circ \circ \circ \end{array}\right)$

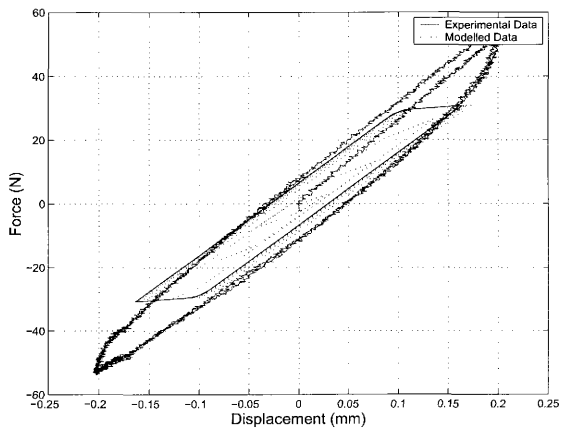


Fig. 23. Comparison of Experimental and Theoretical Force vs. Displacement Response of Experimental System with Four SMA Tube Springs $\left(\begin{array}{c} \circ \circ \\ \circ \circ \end{array}\right)$

pose of this investigation was to determine what performance might be expected out of this system and in what configuration the system might perform best.

Figure 24 shows the effect of varying the amplitude of base excitation on transmissibility of the SMA spring-mass system. These results are shown for a mass of 1 kg , an SMA spring configuration of two upper SMA springs and two lower SMA springs, and a pre-compression of 1 mm for all the springs. At lower amplitude of base excitation, the SMA spring-mass system exhibits resonance at a frequency of approximately 66 Hz , similar to the transmissibility of a linear system which is shown in Figure 24 by the line labelled "analytical." This can be explained by looking at the force-displacement diagram for one of the SMA springs, as shown in Figure 25. For an excitation amplitude of 0.1 g , it is observed that after a few loading cycles the SMA spring repeatedly loads and unloads along a path having a stiffness of approximately 43 KN/m , giving a combined total stiffness of approximately 172 KN/m . For a mass of 1 kg , this equates to a natural frequency of approximately 66 Hz . As the excitation amplitude increases, the decrease in stiffness and hysteresis of the SMA's pseudoelasticity begins to contribute to a reduction in the resonant amplitude of the system. Figure 26 gives the force-displacement history for an excitation amplitude equal to 2.0 g at the natural frequency. A wider hysteresis loop is observed due to increased phase transformation, which is a result of higher excitation amplitude, and results in a lower transmissibility (see Figure 24). Figure 27 shows the system response (displacement history) for 0.1 g excitation amplitude at resonance, and Figure 28 shows the system response for 3.0 g excitation amplitude at resonance. These two figures illustrate the reduction in transmissibility resulting from an increase in the loading on the system. From these results, it can be surmised that the greatest benefit of SMA pseudoelasticity can be gained for this system under higher loading levels and near the resonant frequency of the system. It is also important to understand that

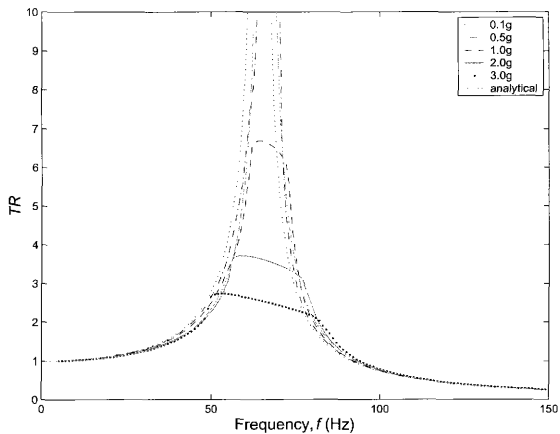


Fig. 24. Transmissibility of SMA Spring-Mass System with Different Amplitude of Base Excitation for 1 kg Mass

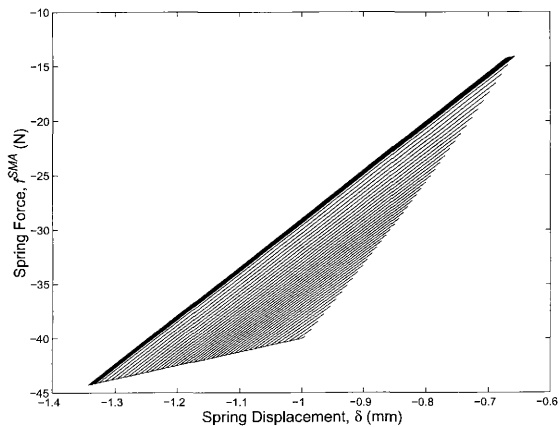


Fig. 25. Force-Displacement Response for an SMA Spring for the System with 1 kg Mass and 0.1 g Excitation Amplitude

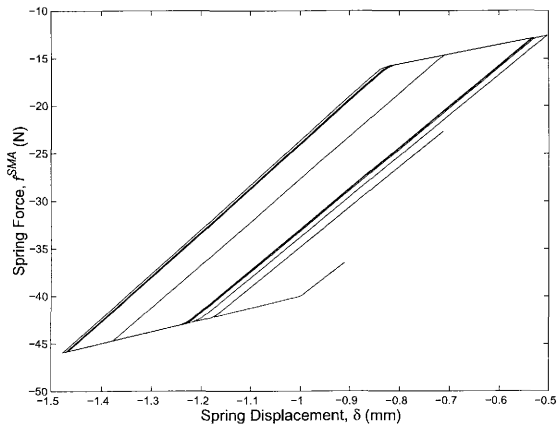


Fig. 26. Force-Displacement Response for an SMA Spring for the System with 1 kg Mass and 2.0 g Excitation Amplitude

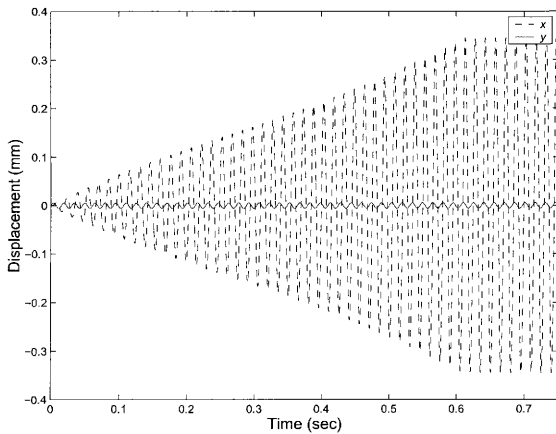


Fig. 27. System Response at Resonance for 1 kg Mass and 0.1 g Excitation

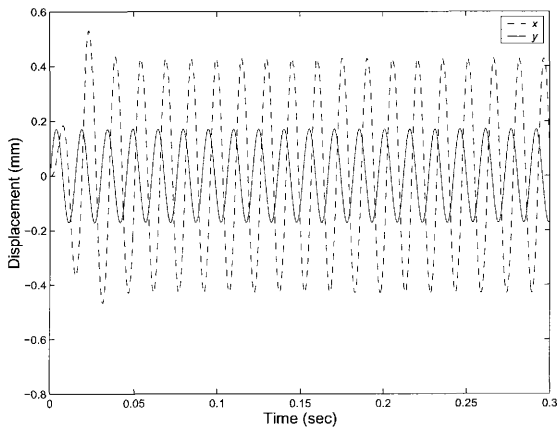


Fig. 28. System Response at Resonance for 1 *kg* Mass and 3.0 *g* Excitation

in order to lower the transmissibility at resonance, the SMA springs should undergo large amplitude displacement that will result in phase transformation. This will allow the system to operate with a lowered effective spring stiffness, due to the pseudoelastic effect, and will allow the inherent hysteresis present in the SMAs to provide energy dissipation. In other words, SMA force-displacement response should be as close as possible to the major loop behavior discussed earlier in order to have the most effective vibration isolation. However, it should be noted that at frequencies much greater than resonance where, in general, the amplitude of vibration is less, the SMAs function more like a linear spring with no damping. At these high frequencies the system dynamics allow for significant reductions in transmissibility, as shown in Figure 29, since the hysteretic damping is not present to adversely affect the transmissibility at these conditions. This is beneficial because it allows the SMA vibration isolation device to have off-peak transmissibility similar to a system with no damping while near the resonant frequency the device's hysteresis will act to reduce resonant amplitude. The effect is that damping is available only when needed and the system damping is not detrimental to off-peak transmissibility as seen in traditional dampers.

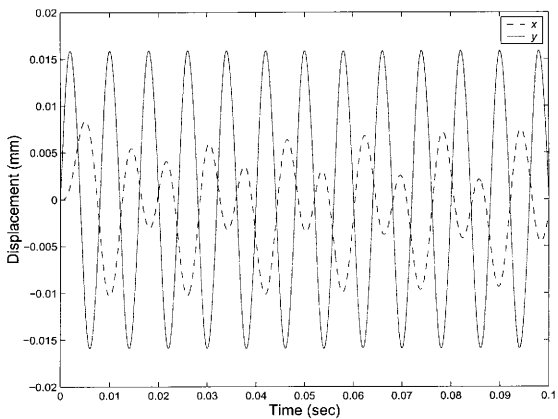


Fig. 29. System Response for 1 kg Mass, 4 SMA Tube Springs, and 1.0 g Excitation Showing Reduction in Transmissibility (125 Hz)

CHAPTER VI

EXPERIMENTAL RESULTS

During the course of this work, several series of experiments were undertaken. These included both standard mechanical tests to calibrate the simplified pseudoelastic model as mentioned earlier and vibration testing to investigate the effect of pseudoelastic components on the response of a dynamic system. The mechanical tests were conducted using the facilities of the Material Testing Laboratory in the Department of Aerospace Engineering at Texas A&M University. The vibration testing was conducted at the Air Force Research Laboratory under the supervision of Dr. Benjamin Kyle Henderson at Kirtland Air Force Base, New Mexico.

A. Vibration Testing of SMA Based Isolation Device

In order to determine what effect the use of pseudoelastic SMA springs would have on a dynamic system, the experimental system as described previously was subjected to a series of experiments on a vibration shaker table at the Air Force Research Laboratory. The excitation during the testing was provided by a VTS-100 electromagnetic shaker and accompanying power amplifier controlled by a Hewlett-Packard 35665A Dynamic Signal Analyzer. Dynamic excitation was measured using two PCB 336C04 accelerometers, with one located on the shaker table and the other located on the SMA spring-mass system. Constant acceleration amplitude frequency sweeps were used as the input waveform and were controlled via a feedback loop using the accelerometer on the shaker table as the input source. Output acceleration was also measured by the signal analyzer and the ratio of the magnitude of the output to the input accelerations was processed to create a frequency domain transfer function for the system. The shaker configuration with the SMA spring-mass system attached is

shown in Figure 30. Figure 31 shows the experiment attached to the shaker assembly as tested at the Air Force Research Laboratory, and Figure 32 shows the entire shaker assembly with the experiment attached.

During the experiments, several of the parameters were varied to determine their effect on the behavior of the system. The number of SMA compression springs, the mass being isolated and the loading input into the system were all varied following the test matrix presented in Table II. Also of interest was determining the effect of changes in the pre-compression of the SMA springs on the dynamic response of the system. Of specific interest was whether it would be possible to modify the system response by adjusting the degree of transformation achieved in the SMA springs. Since the amplitude of motion for this series of tests was relatively small compared to the undeformed length of the SMA springs, the degree of transformation was most influenced by the amount of pre-compression placed on the springs. After setting the pre-compression, the SMA springs would operate in small minor loop hysteresis cycles about that point without much deviation. Naturally, had the loading amplitude been greater, this would not necessarily be true. However, for this system it was possible to manipulate the degree of transformation of the SMA springs by adjusting the pre-compression. As noted in Table II, two different amounts of pre-compression were tested, 20% and 26% reduction in length compared to the original undeformed length. Length, when referring to pre-compression, refers to the transverse axis of the SMA tube, not the longitudinal axis. Testing of Cases 1-8 were all performed at 20% pre-compression levels. Cases 9 and 10 were performed at 26% pre-compression levels, and the results of this series of tests were then compared to the corresponding results from Cases 1 and 6.

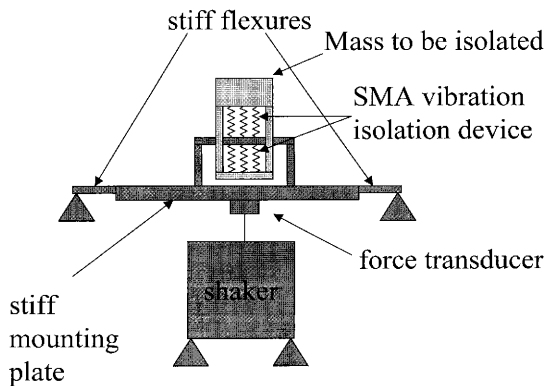


Fig. 30. Schematic of Shaker and SMA Spring-Mass Isolation System as Tested

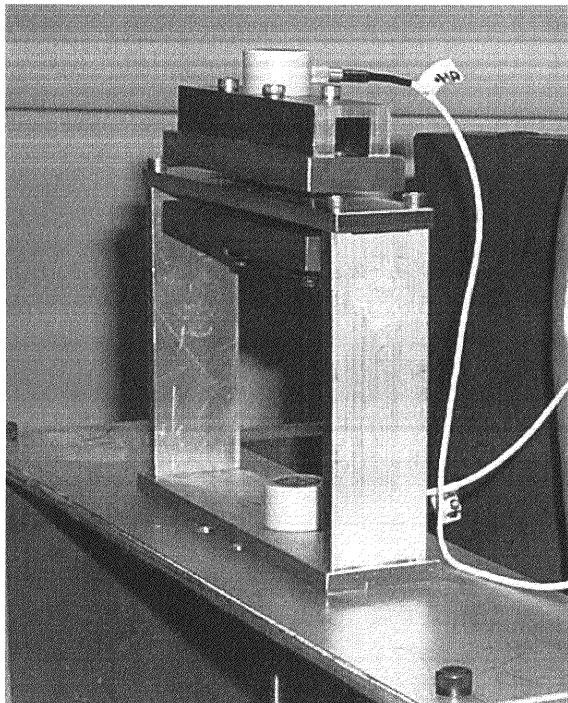


Fig. 31. Picture of SMA Spring-Mass Isolation Experiment Attached to Shaker Table

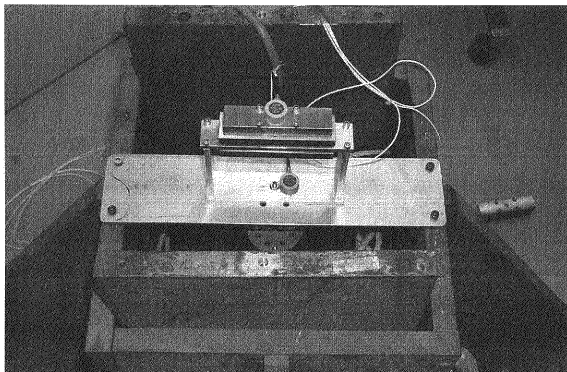


Fig. 32. Picture of Shaker Assembly with Experiment Attached

Table II. Test Matrix for SMA Spring-Mass System

Case Number	Mass (kg)	Number of Springs		Pre-Compression of SMA Springs		Loading (g's)			
		4	6	20%	26%	1/4	1/2	3/4	1
1	0.5	✓		✓		✓	✓	✓	✓
2	0.8	✓		✓		✓	✓	✓	✓
3	1.0	✓		✓		✓	✓	✓	✓
4	1.2	✓		✓		✓	✓	✓	✓
5	1.5	✓		✓		✓	✓	✓	✓
6	0.5		✓	✓		✓	✓	✓	✓
7	0.8		✓	✓		✓	✓	✓	✓
8	1.0		✓	✓		✓	✓	✓	✓
9	0.5	✓			✓	✓	✓		
10	0.5		✓		✓	✓	✓		

B. Results From Vibration Testing of SMA Based Isolation Device

Results from this series of experiments are shown in Figures 33–40. Figures 33–37 show the results for two pair of SMA springs, or four total, and Figures 38–40 show the results for three pair of SMA springs, or six total.

1. Effect of Changes in Loading on System Response

For Figures 33, 34, 35, 36 and 37, where four SMA springs were used, the mass is increased for each successive figure. It should be noted that between testing for Case 2 (Figure 34) and Case 3 (Figure 35), the experiment was reassembled and as a result the same level of pre-compression was not achieved for all of the cases where four SMA springs were used. This is evident by comparing Figure 34 and Figure 35, where the increase in mass should result in a decrease in resonant frequency and does not. However, if Cases 1 and 2 and Cases 3, 4, and 5 are taken as individual series of tests, then an increase in mass results in a lower resonance frequency, as expected from a simplified linear analysis. Also shown by these experiments is, for a constant mass, an additional decrease in resonant frequency as the loading on the system increases. This reduction in frequency can be as much as 25% (Figure 37) but is usually in the range of 5%–10% (Figures 35 and 36). Accompanying the reduction in resonant frequency, there is also a consistent reduction in the magnitude of the resonant peak on the order of 30% (Figures 35, 36 and 37). These reductions can be attributed to the non-linear, hysteretic behavior of the SMA springs and would not be seen in a similar linear system. The same trends as discussed above are seen in Figures 38, 39 and 40 for the experimental system with six SMA springs. Again there is the expected decrease in resonant frequency for increasing mass. Similar to the results from the system using four springs, there is also a reduction in resonant frequency as the loading applied to

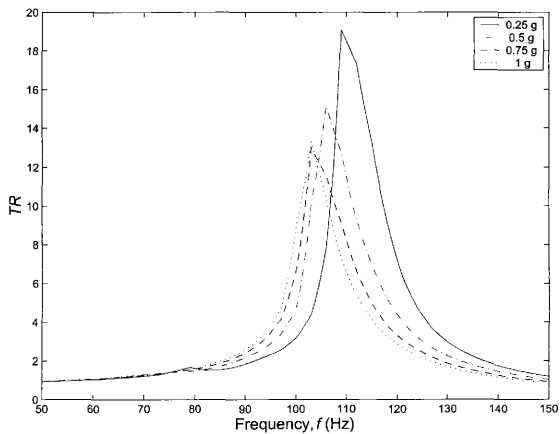


Fig. 33. Transmissibility for Case 1 (∞)

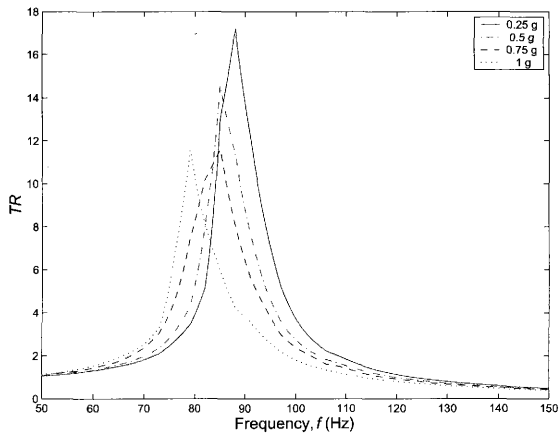


Fig. 34. Transmissibility for Case 2 $\left(\frac{\infty}{\infty}\right)$

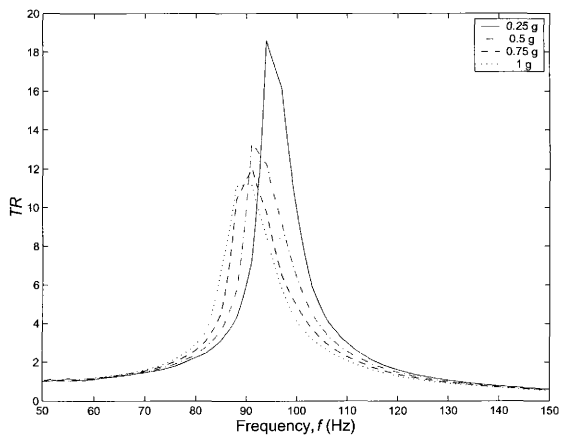


Fig. 35. Transmissibility for Case 3 (∞)

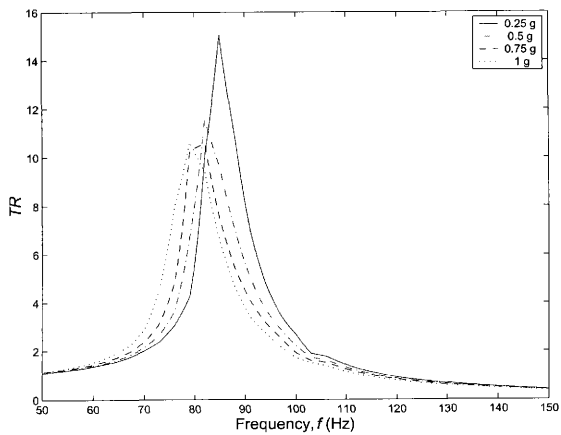


Fig. 36. Transmissibility for Case 4 $\left(\begin{array}{c} \circ \\ \circ \end{array}\right)$

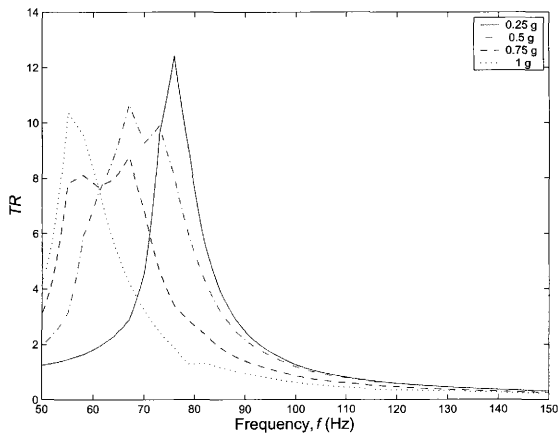


Fig. 37. Transmissibility for Case 5 ($\left(\begin{smallmatrix} \circ & \circ \\ \circ & \circ \end{smallmatrix}\right)$)

the system increases. From Figures 38, 39 and 40 it can be seen that this reduction in resonant frequency is also on the order of 5%–10%. Accompanying this reduction in resonant frequency is a reduction in the resonant amplitude as seen before. For Figure 40, this reduction is approximately 10%. However, for Figures 38 and 39 the reduction in resonant amplitude is much greater, on the order of 30%–35%.

2. Effect of Changes in SMA Spring Pre-Compression on System Response

Referring to Figure 8, it is evident that changes in spring displacement will result in changes in the stiffness of the spring. However, given the non-linear, hysteretic behavior of the pseudoelastic response of SMAs, it was unclear what effect this would have on the response of the system. Therefore, experiments were conducted in which the pre-compression of the SMA springs was changed while all other system parameters were held constant. The results of these tests are presented in Figures 41, 42, 43 and 44. Figures 41 and 42 show the effect of higher pre-compression for a four spring system under 1/4 g and 1/2 g loading conditions, respectively. As shown, increasing the pre-compression results in an increase of resonant frequency by approximately 10%–12%. Figures 43 and 44 show the similar results for a six spring system under the same loading conditions. However for this case, the increase in resonant frequency is approximately 35%–40% for the same increase in pre-compression. As shown, the effect of increasing the pre-compression was an increase in the system stiffness for all cases, with a substantially larger increase seen in the six spring system as compared to the four spring system due to the additional stiffness provided by the greater number of springs.

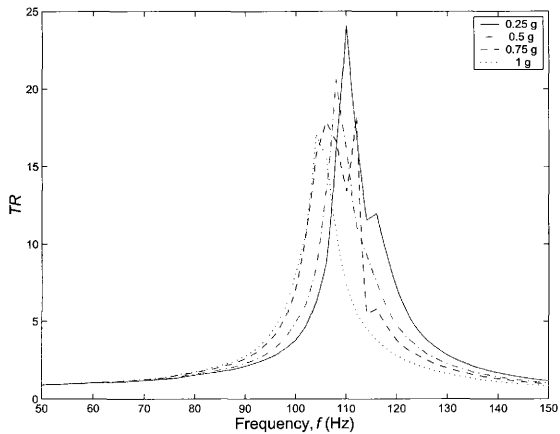


Fig. 38. Transmissibility for Case 6 $\left(\begin{array}{ccc} \circ & \circ & \circ \\ \circ & \circ & \circ \end{array}\right)$

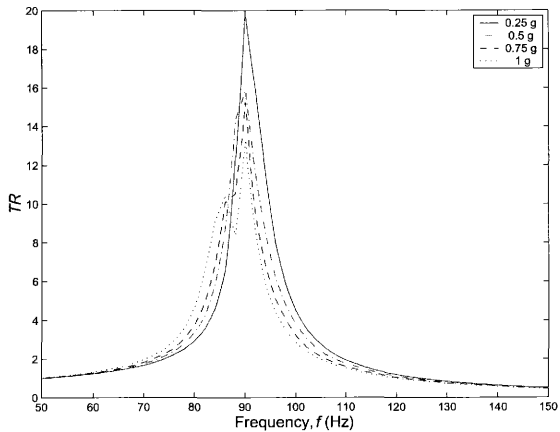


Fig. 39. Transmissibility for Case 7 $\left(\begin{array}{ccc} \circ & \circ & \circ \\ \circ & \circ & \circ \end{array} \right)$

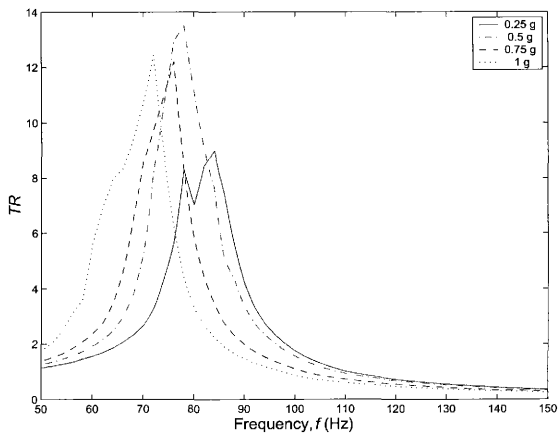


Fig. 40. Transmissibility for Case 8 $\left(\begin{array}{c} \text{○○○} \\ \text{○○○} \end{array} \right)$

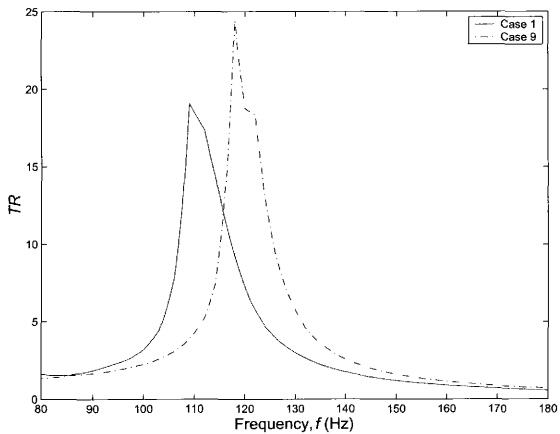


Fig. 41. Transmissibility for Case 1 $\left(\frac{\infty}{\infty}\right)$ and Case 9 $\left(\frac{\infty}{\infty}\right)$, $1/4 g$ Loading

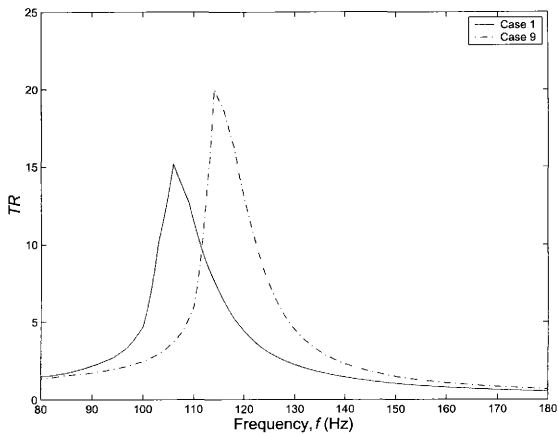


Fig. 42. Transmissibility for Case 1 $\left(\frac{\infty}{\infty}\right)$ and Case 9 $\left(\frac{\infty}{\infty}\right)$, $1/2 g$ Loading

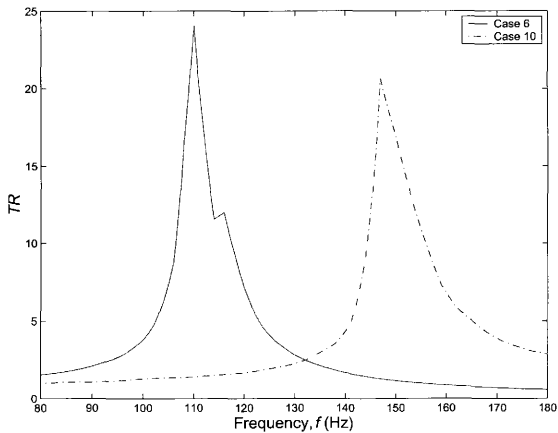


Fig. 43. Transmissibility for Case 6 $\left(\begin{array}{ccc} \circ & \circ & \circ \\ \circ & \circ & \circ \end{array}\right)$ and Case 10 $\left(\begin{array}{ccc} \circ & \circ & \circ \\ \circ & \circ & \circ \end{array}\right)$, $1/4 g$ Loading

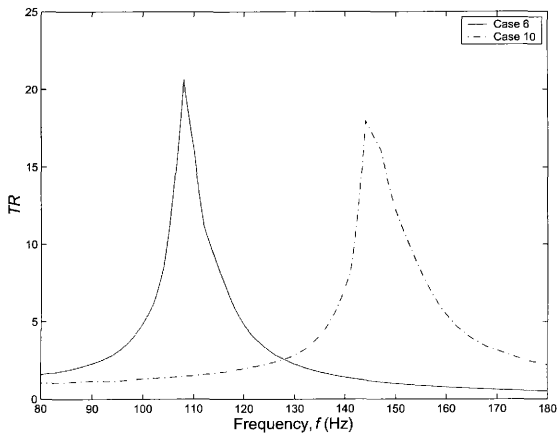


Fig. 44. Transmissibility for Case 6 $\left(\begin{smallmatrix} \circ & \circ & \circ \\ \circ & \circ & \circ \end{smallmatrix}\right)$ and Case 10 $\left(\begin{smallmatrix} \circ & \circ & \circ \\ \circ & \circ & \circ \end{smallmatrix}\right)$, $1/2 g$ Loading

CHAPTER VII

COMPARISON OF EXPERIMENTAL RESULTS AND THEORY

In this section, theoretical predictions of the system response of the SMA-based isolation system will be compared with results obtained from the experimental analysis of the system.

A study of the experimental results and the results predicted from the material model and simulation presented in this work indicate that there is significant agreement between the two and the effect of the pre-compression is shown to drastically effect the response of the system. Based on the results presented in the previous chapter, the pre-compression can greatly shift the resonant frequency of the system. This is shown in the comparison of Cases 9 and 10 and Cases 6 and 11. It is also shown in the difference in resonant frequency for Case 2 and Case 3, albeit inadvertently. Inadequacies in the experimental design prevented absolute certainty as to the amount of pre-compression. Although every effort was made to ensure the correct amount of pre-compression had been applied to the system, it is evident that even the slightest change in the pre-compression will alter the system response greatly.

In comparing experimental and theoretical results, it was found that a correlation could be made if the pre-compression value given to the numerical simulation was set equal to 2.25 mm, or roughly 37.5% of the total transverse displacement of the tube. The amount of pre-compression for Cases 9 and 10 was also adjusted, to 2.3 mm, in order to agree with experiment. Presented in Figures 45 through 48 are the results of the numerical simulation for Cases 9 and 10 and Cases 2, 7, and 8, along with the experimental results for the respective cases. For all cases, the resonant amplitude of the experimental data is less than that for the numerical simulation. Additionally, for every case there is a good correlation between the resonant frequency predicted

by the simulation and the resonant frequency measured during the experiment. For Figure 45, the effect of changes in pre-compression is seen to have dramatic effect in both the experiment and the numerical simulation. For both the experimental data and the simulation results, relatively small increases in the pre-compression are shown to increase the resonant frequency greatly. This is an important result as it shows that SMA based isolation devices lend themselves well to being developed as tuneable isolation devices capable of providing isolation for various conditions and loads.

At frequencies much greater than the resonant frequency, the modelled and experimentally obtained values for transmissibility agree very well. From simulation in this region, it seems that the SMA springs are functioning linearly, that is without transformation. This should prove beneficial as it would prevent the inherent damping present during transformation from degrading the performance of the isolator. Finally, the same trends of decreasing resonant amplitude for increasing loading are seen in both the simulation data and the experimental data. Since simulation of this region indicates that the reduction in amplitude is due to larger deformations of the SMA springs which results in more energy being absorbed by the isolation device. Combined with the observations of nearly linear behavior at frequencies much greater than the resonant frequency, this observation is very important because it indicates that the SMA isolation device will be capable of providing sufficient damping at resonance where high damping is beneficial and will provide minimal damping at higher frequencies where damping degrades isolation performance.

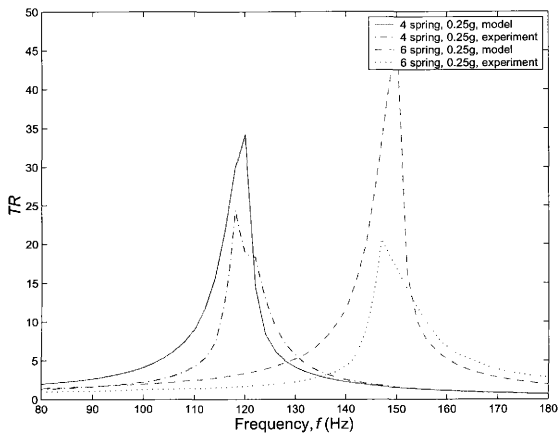


Fig. 45. Comparison of Numerical Simulation with Experimental Results for Case 9 $\left(\begin{smallmatrix} \circ\circ \\ \circ\circ \end{smallmatrix}\right)$ and Case 10 $\left(\begin{smallmatrix} \circ\circ\circ \\ \circ\circ\circ \end{smallmatrix}\right)$

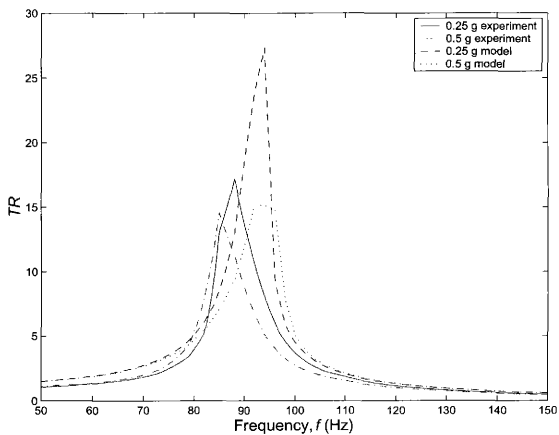


Fig. 46. Comparison of Numerical Simulation with Experimental Results for Case 2
($\begin{pmatrix} \circ & \circ \\ \circ & \circ \end{pmatrix}$)

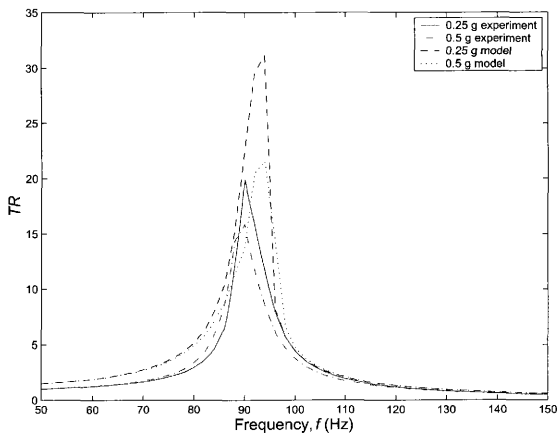


Fig. 47. Comparison of Numerical Simulation with Experimental Results for Case 7



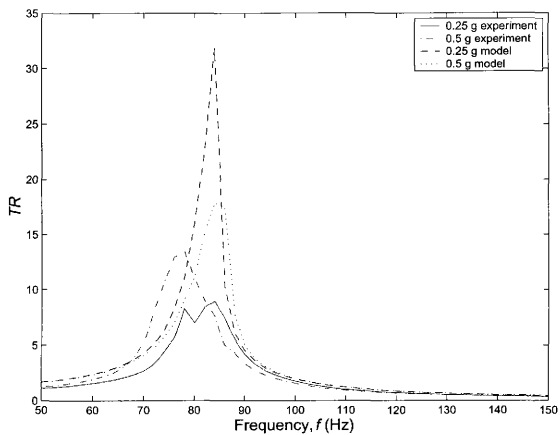


Fig. 48. Comparison of Numerical Simulation with Experimental Results for Case 8



CHAPTER VIII

DISCUSSION OF RESULTS AND FUTURE WORK

This chapter will discuss several of the issues that have arisen as a result of this work and will provide directions for future work in this area. Additionally, suggestions on how to improve the correlation of these results, through modification of both the experiment and theory, will be presented where appropriate.

A. Comments on the Differences Observed Between Experimental Results and Expected Performance

It is evident that the amount of pre-compression imposed on the SMA springs has a large and direct effect on the system response. It is also evident that the design of the experiment used in this work allows for poor accuracy and a lack of repeatability with respect to specifying the pre-compression. After comparing the experimental results with the results from the numerical simulation, it is believed that much better agreement between the two could be obtained if the pre-compression in the springs was known precisely and either specified exactly for the experiment, or at the very least, accurately measured during experimentation for use in the simulation. Additionally, a redesign of the experiment would ensure that there would be no possible contact between any of the moving parts, thereby ensuring that the SMA spring response is being measured correctly. Based on these reasons, it is felt that a redesign of the experiment would provide the best results.

Possible alternatives to the current design include a design where the springs work in tension and compression, thus eliminating the whole necessity of pre-compression. In this case, the mass being isolated would provide the force to transition the SMA material into the pseudoelastic region where the input vibration would cause oscil-

lations about the static displacement point. Another option is to develop a new configuration entirely, eliminating the tubes from the experiment and replacing them with a different type of spring device such as a helical spring or leaf spring made from SMA material.

With regards to the model, there are a few areas that can be addressed in an effort to improve agreement with experimental results. The numerical formulation is idealized and does not take into account any friction between the different parts of the experiment. This area may be addressed rather easily and could provide immediate benefit. The addition of any friction elements would also allow for numerical investigation into the effects of additional damping in the system.

B. Future Work

While this investigation has provided a solid foundation with which to investigate the application of pseudoelastic SMA for use as vibration isolators, much work has yet to be done. The chief among these is a furthering of the experimental work presented here. A comprehensive investigation into different spring designs and into which designs provide the most efficient implementation of the damping available in the SMA pseudoelastic effect would contribute greatly to the understanding of the impact of SMA based components on dynamic systems. Additionally, an investigation into the performance of various shape memory alloys and the effect of varying compositions should be undertaken.

In the area of computational prediction of system response, there are several items that can also be addressed. Accounting for the non-isothermal nature of the SMA phase transition might result in more accurate modelling of the system, even though no change in temperature was detected during either the quasi-static or dy-

dynamic testing presented in this work. While a change in temperature is often associated with rapid stress induced phase transition in SMAs, the lack of temperature change noted in this work is attributed to the large amount of highly conductive surface area in contact with other conductive surfaces in the experiment and the limited amount of material undergoing complete transformation due to the tubular shape of the SMA spring devices.

A redesign of the experiment should be implemented to address the following areas, SMA tube spring failure and better exploitation of the SMA pseudoelastic response. Several of the SMA tube springs experienced structural failure during testing attributed to stress concentrations resulting from the geometric boundary conditions on the tubes that were further exacerbated by inconsistencies or flaws in the material. A full finite element analysis of the experiment would help to redesign the current experiment to avoid these issues. Additionally, various other SMA element configurations should be investigated in an effort to achieve a response similar to the one dimensional pseudoelastic behavior of SMA, such that more exploitation of the decrease in component stiffness during pseudoelastic transformation could be made. Furthermore, full finite element analysis of both the SMA tube spring and the experimental setup would be able to assist in the redesign suggested earlier. This effort should have the goal of determining if there are any dynamic modes or other interactions present due to geometric constraints that can be avoided by simple design changes. Finally, it may be possible to implement a solution to the dynamic system, perhaps using a finite element solution method, that uses a more sophisticated SMA material model to provide a more accurate dynamic response of both the SMAs and the system.

CHAPTER IX

CONCLUSIONS

This work has presented several achievements with regard to establishing the suitability of pseudoelastic SMAs as vibration isolation devices. The development of a simplified material model for the predication of the non-linear, hysteretic behavior associated with SMAs has been developed and presented in terms of modelling the force-displacement relationship of a pseudoelastic SMA spring. Additionally, this material model has been integrated with the numerical solution of a dynamic system where it provides the non-linear, hysteretic and history dependent response of the SMA springs used to provide the restoring force to an SMA based spring mass system. This connection provides the basis for a flexible software tool that can be used to model SMA based isolation systems of various configurations under diverse loading conditions. This software has been utilized to study the theoretical behavior of an SMA based vibration isolation device.

In addition to the theoretical work summarized here, an experimental effort has been undertaken to expand the understanding and knowledge of a dynamic system based on SMAs. This effort included the design and testing of a prototype of an SMA based isolation device using tubular shaped SMA isolators. Numerous quasi-static tests were used to characterize the SMA tubes used as springs and to explore the response of the entire isolation system. Results of this testing, and the associated modelling, have shown that large amplitude deflections are necessary in order for the SMA isolators to exhibit the non-linear, hysteretic behavior which inherent in SMA pseudoelasticity. Vibration testing of this device has provided insight into the behavior of SMAs under dynamic loading. Reductions in resonant amplitude and frequency were noted as the loading amplitude increased and this behavior is attributed

to the pseudoelastic behavior of the SMAs. These larger amplitudes of displacement at higher loading levels allow for larger minor loop pseudoelastic transformation of the isolators which results in an increase in the energy dissipated by the isolation device. Additionally, it has been shown that at frequencies much greater than the resonant frequency, the hysteretic behavior is less pronounced due to lower displacement amplitudes. This allows the system to have much lower transmissibility since the damping is not present.

Correlation between the numerical simulation and the experiments has also been made and while there were differences between the experimental results and the theoretical results, sufficient correlation was made to validate both the numerical simulation and the premise of using SMAs as vibration isolation devices. Additionally, much insight has been gained into how to model the effect of SMA pseudoelasticity on dynamic systems and how best to experimentally verify these effects.

While this study has by no means finished the investigation of the applicability of SMAs to vibration isolation, it has provided a strong foundation for this work to progress. Through this work, experimental experience has been developed with relation to the implementation of SMAs in dynamic systems. Additionally, tools have been developed to aid in the theoretical modelling of a variety of applications involving SMAs. Finally, direction has been provided for future work, specifically in the areas of improving the experimental setup and numerical simulation. As shown in this work, SMAs have the potential to be successfully applied to the many different areas of vibration isolation.

REFERENCES

- [1] L. N. Dumas and A. L. Walton, "Faster, better, cheaper: An institutional view," *Acta Astronautica*, vol. 47, no. 2-9, pp. 607-621, 2000.
- [2] E. K. Casani, "Reduced cost and increased capability through technology in the new millennium," *Acta Astronautica*, vol. 39, no. 1-4, pp. 153-160, 1996.
- [3] S. Ashley, "Bringing launch cost down to earth," *Mechanical Engineering*, vol. 120, no. 10, pp. 62-68, 1998.
- [4] A. S. Bicos, C. D. Johnson, and L. P. Davis, "Need for and benefits of launch vibration isolation," in *Proceedings of the SPIE*, 1997, vol. 3045, pp. 14-19.
- [5] D. L. Edberg, C. D. Johnson, L. P. Davis, and E. R. Fosness, "On the development of a launch vibration isolation system," in *Proceedings of the SPIE*, 1997, vol. 3045, pp. 31-37.
- [6] D. L. Edberg, B. Bartos, J. Goodding, P. Wilke, and T. Davis, "Passive and active launch vibration studies in the LVIS program," in *Proceedings of the SPIE*, 1998, vol. 3327, pp. 411-422.
- [7] P. S. Wilke, C. D. Johnson, and E. R. Fosness, "Payload isolation system for launch vehicles," in *Proceedings of the SPIE*, 1997, vol. 3045, pp. 20-30.
- [8] P. S. Wilke, C. D. Johnson, P. Grosserode, and D. Sciulli, "Whole spacecraft vibration isolation for broadband attenuation," in *Aerospace Conference Proceedings*, 2000, vol. 4, pp. 315-321.

- [9] C. D. Johnson, P. S. Wilke, and P. J. Grosserode, "Whole-spacecraft vibration isolation system for the GFO/Taurus mission," in *Proceedings of the SPIE*, 1999, vol. 3672, pp. 175–185.
- [10] J.-H. Yu, E. Postrekin, K. B. Ma, and W.-K. Chu, "Vibration isolation for space structures using lts-magnet interaction," *IEEE Transactions on Applied Superconductivity*, vol. 9, no. 2, pp. 908–910, 1999.
- [11] R. G. Cobb, J. M. Sullivan, A. Das, L. P. Davis, T. T. Hyde, T. Davis, Z. H. Rahman, and J. T. Spanos, "Vibration isolation and suppression system for precision payloads in space," *Smart Materials and Structures*, vol. 8, pp. 798–812, 1999.
- [12] B. K. Wada, Z. Rahman, R. Kedikian, and C.-P. Kuo, "Vibration isolation, suppression and steering (VISS)," *Journal of Intelligent Materials Systems and Structures*, vol. 7, pp. 241–245, 1996.
- [13] E. H. Anderson, J. P. Fumo, and R. S. Erwin, "Satellite ultraquiet isolation technology experiment (SUITE)," in *Aerospace Conference Proceedings*, 2000, vol. 4, pp. 299–313.
- [14] Y. C. Yiu and M. E. Regelbrugge, "Shape-memory alloy isolators for vibration suppression in space applications," in *36th AIAA/ASME/ASCE/AHS/ASC Structures, Structural Dynamics, and Materials Conference*, 1995, pp. 3390–3398.
- [15] D. Wolons, F. Gandhi, and B. Malovrh, "Experimental investigation of the pseudoelastic hysteresis damping characteristics of nickel titanium shape memory alloy wires," *Journal of Intelligent Material Systems and Structures*, vol. 9, pp. 116–126, 1998.

- [16] R. Fosdick and Y. Ketema, "Shape memory alloys for passive vibration damping," *Journal of Intelligent Systems and Structures*, vol. 9, pp. 854–870, 1998.
- [17] Y. Matsuzaki, T. Kamita, and T. Yamamoto, "Vibration characteristics of shape memory alloys," in *Proceedings of the SPIE*, 1998, vol. 3329, pp. 562–569.
- [18] T. L. Turner, "Dynamic response tuning of composite beams by embedded shape memory alloy actuators," in *Proceedings of the SPIE*, 2000, vol. 3991, pp. 377–388.
- [19] E. J. Graesser and F. A. Cozzarelli, "Shape-memory alloys as new materials for aseismic isolation," *Journal of Engineering Materials*, vol. 117, no. 11, pp. 2590–2608, 1991.
- [20] K. Wilde, P. Gardoni, and Y. Fujino, "Base isolation system with shape memory alloy device for elevated highway bridges," *Engineering Structures*, vol. 22, pp. 222–229, 2000.
- [21] P. Thomson, G. J. Balas, and P. H. Leo, "The use of shape memory alloys for passive structural damping," *Smart Materials and Structures*, vol. 4, no. 1, pp. 36–41, March 1995.
- [22] Z. C. Feng and D. Z. Li, "Dynamics of a mechanical system with a shape memory alloy bar," *Journal of Intelligent Material Systems and Structures*, vol. 7, pp. 399–410, 1996.
- [23] L. L. Beranek and I. L. Vér, Eds., *Noise and Vibration Control Engineering*, New York:John Wiley and Sons, 1992.
- [24] C. M. Harris, Ed., *Shock and Vibration Handbook*, New York:McGraw-Hill, 1996.

- [25] H. Funakubo, Ed., *Shape Memory Alloys*, New York:Gordon and Breach Science Publishers, 1987.
- [26] C.M. Wayman, "Phase transformations, nondiffusive," in *Physical Metallurgy*, R.W. Cahn and P. Haasen, Eds., pp. 1031-1074. New York:Elsevier Science Publishing Company, 1983.
- [27] S. G. Shu, D. C. Lagoudas, D. Hughes, and J. T. Wen, "Modeling of a flexible beam actuated by shape memory alloy wires," *Shape Memory Alloy Material Structures*, vol. 6, pp. 265-277, 1997.
- [28] K. Otsuka and C. M. Wayman, Eds., *Shape Memory Materials*, New York:Cambridge University Press, 1999.
- [29] L. J. Garner, L. N. Wilson, and D. C. Lagoudas, "Development of a shape memory alloy actuated biomimetic vehicle," *Smart Structures and Materials*, vol. 9, no. 5, pp. 673-683, 2000.
- [30] O. K. Redonitis, D. C. Lagoudas, L. Garner, and N. Wilson, "Experiments and analysis of an active hydrofoil with SMA actuators," in *36th AIAA Aerospace Sciences Meeting*, 1998.
- [31] C. Liang, F. M. Davidson, L. M. Schetky, and F. K. Straub, "Applications of torsional shape memory alloy actuators for active rotor blade control: opportunities and limitations," in *Proceedings of the SPIE*, 1996, vol. 2717, pp. 91-100.
- [32] Z. Chaudry and C. A. Rogers, "Bending and shape control of beams using sma actuators," *Journal of Intelligent Material Systems and Structures*, vol. 2, no. 4, pp. 581-602, 1991.

- [33] A. Bhattacharyya and D. C. Lagoudas, "Modeling of thin layer extensional thermomechanical actuators," *International Journal of Solids and Structures*, vol. 35, no. 3-4, pp. 331-362, 1998.
- [34] S. Miyazaki, T. Imai, Y. Igo, and K. Otsuka, "Effect of cyclic deformation on the pseudoelasticity characteristics of Ti-Ni alloys," *Metallurgical Transactions*, vol. 42, no. 7, pp. 115-120, 1997.
- [35] H. Ozdemir, "Nonlinear transient dynamic analysis of yielding structures," Ph.D. dissertation, University of California at Berkeley, Berkeley, CA, 1976.
- [36] M. Achenbach, T. Atanochovic, and I. Muller, "A model for memory alloys in plane strain," *International Journal of Solids and Structures*, vol. 22, no. 2, pp. 171-193, 1986.
- [37] R. Aberayratne and J. K. Knowles, "Dynamics of propagating phase boundaries: Thermoelastic solids with heat conduction," *Archive for Rational Mechanics and Analysis*, vol. 126, no. 3, pp. 203-230, 1994.
- [38] D. C. Lagoudas, Z. Bo, and M. A. Qidwai, "A unified thermodynamic constitutive model for sma and finite element analysis of active metal matrix composites," *Mechanics of Composite Materials and Structures*, vol. 3, pp. 153-179, 1996.
- [39] D. C. Lagoudas and Z. Bo, "Thermomechanical modeling of polycrystalline SMAs under cyclic loading, Part II: Material characterization and experimental results for a stable transformation cycle," *International Journal of Engineering Science*, vol. 37, pp. 1141-1173, 1999.
- [40] L. C. Brinson, "One-dimensional constitutive behavior of shape memory alloys: Thermomechanical derivation with non-constant material functions and rede-

- finned martensite internal variable,” *Journal of Intelligent Material Systems and Structures*, vol. 4, pp. 229–242, 1993.
- [41] C. Liang and C. A. Rogers, “One-dimensional thermomechanical constitutive relations for shape memory materials,” in *31st AIAA/ASME/ASCE/AHS/ASC Structures, Structural Dynamics and Materials Conference*, 1990, pp. 16–28.
- [42] K. Tanaka, “A thermomechanical sketch of shape memory effect: One-dimensional tensile behavior,” *Res Mechanica*, vol. 18, pp. 251–263, 1986.
- [43] Y. Sato and K. Tanaka, “Estimation of energy dissipation in alloys due to stress-induced martensitic transformation,” *Res Mechanica*, vol. 23, pp. 381–392, 1988.
- [44] E. Patoor, A. Eberhardt, and M. Berveiller, “Potentiel pseudoélastique et plasticité de transformation martensitique dans les mono et polycristaux métalliques,” *Acta Metallurgica*, vol. 35, pp. 2779–2789, 1987.
- [45] F. Falk, “Pseudoelastic stress strain curves of polycrystalline shape memory alloys calculated from single crystal data,” *International Journal of Engineering Science*, vol. 27, pp. 277, 1989.
- [46] F. Preisach, “Über die magnetische nachwirkung,” *Zeitschrift für Physik*, vol. 94, pp. 277–302, 1935.
- [47] I. Mayergoyz, *Mathematical Models of Hysteresis*, New York:Springer-Verlag, 1991.
- [48] H. T. Banks, A. J. Kurdila, and G. V. Webb, “Identification of hysteretic control influence operators representing smart actuators: Formulation,” Tech. Rep. CRSC-TR96-14, Center for Research in Scientific Computation, North Carolina State University, Raleigh, NC, 1996.

- [49] H. T. Banks, A. J. Kurdila, and G. V. Webb, "Identification of hysteretic control influence operators representing smart actuators: Convergent approximations," Tech. Rep. CRSC-TR97-7, Center for Research in Scientific Computation, North Carolina State University, Raleigh, NC, 1997.
- [50] G. V. Webb, "Adaptive identification and compensation for a class of hysteresis operators," Ph.D. dissertation, Texas A&M University, College Station, TX, 1998.
- [51] G. V. Webb, A. J. Kurdila, and D. C. Lagoudas, "Hysteresis modeling of SMA actuators for control applications," *Journal of Intelligent Material Systems and Structures*, vol. 9, no. 6, pp. 432-448, 1998.
- [52] Z. Bo and D. C. Lagoudas, "Thermomechanical modeling of polycrystalline SMAs under cyclic loading, Part IV: Modeling of minor hysteresis loops," *International Journal of Engineering Science*, vol. 37, pp. 1205-1249, 1999.
- [53] The Mathworks Incorporated, "MATLAB," Natick, MA, 1999.
- [54] N. M. Newmark, "A method of computation for structural dynamics," *Journal of Engineering Mechanics Division*, ASCE, vol. 85, pp. 67-94, 1959.
- [55] J. N. Reddy, *An Introduction to the Finite Element Method*, New York:McGraw-Hill, 1993.
- [56] T. J. R. Hughes, *The Finite Element Method*, Englewood Cliffs, NJ:Prentice-Hall, Inc., 1987.

APPENDIX A

MECHANICAL DRAWINGS FOR SMA VIBRATION ISOLATION PROTOTYPE

The following pages contain the mechanical drawings used in the manufacturing of the prototype SMA based vibration isolation device as described earlier in this work.

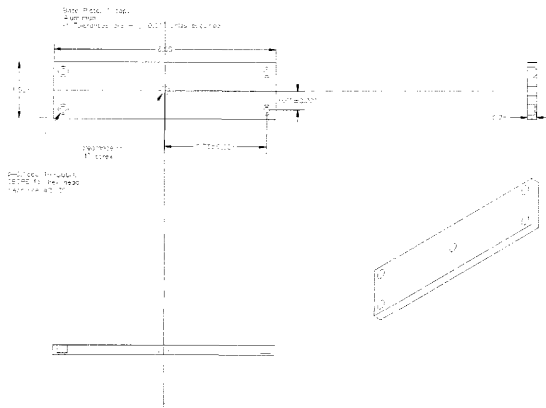


Fig. 49. Drawing for Experiment Base

APPENDIX B

MATLAB CODE FOR VIBRATION ISOLATION SIMULATION

The following pages contain the MATLAB code for the simplified material model discussed in Chapter III and the numerical simulation discussed in Chapter V, which together allow for the simulation of dynamic systems with integral SMA components.

Simplified Material Model Code

The following code is the implementation of the simplified material model for SMA pseudoelasticity as discussed in Chapter III.

```
function [force, ts, h_data] = ...
smasintube(value, rate, tslast, m_data, h_data)
% Simple SMA model for tubes (compression only)
% displacement mode, revision 1
% 5 Feb 2001
% JJ Mayes

% takes in strain and outputs stress

% using linear relationship between transformation strain
% and strain
% using linear relationship between stress and strain
% calculates stiffness using above relationships

% Works for major and minor loops

% Inputs

% value: current value of strain
% rate: current rate of strain
% tslast: last value of transformation strain

% m_data(1): first elastic stiffness
% m_data(2): second elastic stiffness
% m_data(3): maximum of transformation strain
% m_data(4): displacement at forward transformation start
% m_data(5): displacement at forward transformation finish
% m_data(6): displacement at reverse transformation start
% m_data(7): displacement at reverse transformation finish
```

```

% m_data(8): force at forward transformation start
% m_data(9): force at forward transformation finish
% m_data(10): force at reverse transformation start
% m_data(11): force at reverse transformation finish
% m_data(12): 1/m_data(3)

% h_data(1): previous minimum value of transformation strain
% h_data(2): previous maximum value of transformation strain
% h_data(3): previous minimum value of displacement
% h_data(4): previous maximum value of displacement
% h_data(5): previous minimum value of force
% h_data(6): previous maximum value of force

% Outputs

% out: the output value of force

% ts: the current value of transformation strain

% calculate the transition points for stress and strain
% based on previous cycle's maximum and minimum values
% transition points 1 and 3 are the only ones that change
% if transformation strain is not 0 or max then the points
% need to be changed
etp1=m_data(4)+h_data(1)*m_data(12)*(m_data(5)-m_data(4)); %Ms
stp1=m_data(8)+h_data(1)*m_data(12)*(m_data(9)-m_data(8));
etp3=m_data(7)+h_data(2)*m_data(12)*(m_data(6)-m_data(7)); %As
stp3=m_data(11)+h_data(2)*m_data(12)*(m_data(10)-m_data(11));

% calculate transformation strain, stress and slope
if (value+rate)>=0 % for loading
    if abs(value)<=etp1
        ts=tslast;
        force = sign(value)*(h_data(5)+(abs(value)-h_data(3))*...
            m_data(1)*m_data(2)/(h_data(1)*m_data(12)*...
            (m_data(1)-m_data(2))+m_data(2)));
    elseif abs(value)>etp1 & abs(value)<=m_data(5)
        ts=m_data(3)*(abs(value)-m_data(4))/(m_data(5)-m_data(4));
        if ts<h_data(1)
            ts=h_data(1);
        end
        force=sign(value)*(m_data(8)+(m_data(9)-m_data(8))*...
            (ts/m_data(3)));
    elseif abs(value)>m_data(5)
        ts = m_data(3);
        force=sign(value)*(m_data(9)+(abs(value)-m_data(5))*m_data(2));
    else
        error('Out of range Value, SMA subroutine: Forward Transformation')
    end
    h_data(6)=abs(force);
    h_data(4)=abs(value);

```

```

    h_data(2)=ts;
end
if (value*rate)<0
% for unloading
if abs(value)>=etp3
    ts = tslast;
    force=sign(value)*(h_data(6)+(abs(value)-h_data(4))*...
        m_data(1)+m_data(2)/(h_data(2)*m_data(12)*...
        (m_data(1)-m_data(2))+m_data(2)));
elseif abs(value)<etp3 & abs(value)>=m_data(7)
    ts=m_data(3)*(abs(value)-m_data(7))/(m_data(6)-m_data(7));
    if ts>h_data(2)
        ts=h_data(2);
    end
    force=sign(value)*(m_data(11)+(m_data(10)-m_data(11))*...
        (ts/m_data(3)));
elseif abs(value)<m_data(7)
    ts = 0;
    force=value*m_data(1);
else
error('Out of range Value, SMA subroutine: Reverse Transformation')
end
h_data(5)=abs(force);
h_data(3)=abs(value);
h_data(1)=ts;
end

if (value>=0)
force=0;
end

return

```

Numerical Simulation Code

The following codes are components of the implementation of the numerical simulation as discussed in Chapter V.

Main Program

The following code is the main program and calls the system model to obtain a time history of the behavior of the dynamic system for an individual loading level and frequency. It then takes this data and calculates the transmissibility for the given

conditions and saves the time history and transmissibility data in the files specified.

```
% Main Program for Vibration Isolation Simulation
% Calls system model for specified mass, tube count,
% g loading and frequency values specified below
```

```
mass_values = [1.2];
tube_values = [2];
gload_values = [.1];
freq_values = [50:10:200];

for i = 1:length(mass_values)
for j = 1:length(tube_values)
for k = 1:length(gload_values)
    for l = 1:length(freq_values)

data = model(mass_values(i),tube_values(j),...
gload_values(k),freq_values(l));
```

```
filename = strcat('data\m',...
num2str(mass_values(i)), 't',...
num2str(tube_values(j)),...
'g', num2str(k), 'f',...
num2str(freq_values(l)));
```

```
save(filename, 'data');
```

```
n =length(data);
trans(l) = (norm(data(:,2))/sqrt(n)) / ...
(norm(data(:,5))/sqrt(n));
clear data filename
```

```
end
filename = strcat('data\trans_m',...
num2str(mass_values(i)), 't',...
num2str(tube_values(j)),...
'g', num2str(k));
m = mass_values(i);
t = tube_values(j);
g = gload_values(k);
f = freq_values;
save(filename, 'm', 't', 'g', 'f', 'trans');
```

```
clear trans filename m t f
fprintf('finished with mass %g, tube %g',...
' and gload %g\n', mass_values(i),...
tube_values(j), gload_values(k))
```

```

end
end
end

```

System Model

The following code is the system model and is called by the main program for a given frequency and amplitude. This code calls the Newmark integration subroutine for each time step to determine the dynamic response as a function of time.

```

function data=model(mass,tubecount,gload,freq)
% Model for isolator with tubes using smasimtube
% John Mayes
% 4 May 2001

%%%%%%%%%%%%%%%%%%%%%%%%%%%%%%%%%%%%%%%%%%%%%%%%%%%%%%%%%%%%%%%%%%%%%%%%
% Data Input Section
%%%%%%%%%%%%%%%%%%%%%%%%%%%%%%%%%%%%%%%%%%%%%%%%%%%%%%%%%%%%%%%%%%%%%%%%

%%%%%%%%%%%%%%%%%%%%%%%%%%%%%%%%%%%%%%%%%%%%%%%%%%%%%%%%%%%%%%%%%%%%%%%%
% Simulation Data
%%%%%%%%%%%%%%%%%%%%%%%%%%%%%%%%%%%%%%%%%%%%%%%%%%%%%%%%%%%%%%%%%%%%%%%%
% Enter the maximum time of the simulation (sec):
Time= 1; % seconds
% stability and accuracy parameters for newmark scheme
alpha = 1/2;
gamma = 1/2;
errorfactor = 1e-8;
% time step
tau = 1e-3; %seconds

%%%%%%%%%%%%%%%%%%%%%%%%%%%%%%%%%%%%%%%%%%%%%%%%%%%%%%%%%%%%%%%%%%%%%%%%
% Forcing Function Data
%%%%%%%%%%%%%%%%%%%%%%%%%%%%%%%%%%%%%%%%%%%%%%%%%%%%%%%%%%%%%%%%%%%%%%%%
biasload = 0; % g
vibrationload = gload; % g
%freq = 50; % Hz
% Enter the maximum applied displacement:
ymax= (12*32.2*vibrationload)/((freq*2*pi)^2); % inches
% enter 1 to initialize for gravity and 0 for no initialization
init_for_g = 0;

%%%%%%%%%%%%%%%%%%%%%%%%%%%%%%%%%%%%%%%%%%%%%%%%%%%%%%%%%%%%%%%%%%%%%%%%
% Physical Parameters
%%%%%%%%%%%%%%%%%%%%%%%%%%%%%%%%%%%%%%%%%%%%%%%%%%%%%%%%%%%%%%%%%%%%%%%%

% Enter number of tubes in each direction:

```

```

number_top = tubecount;
number_bot = tubecount;
Dia_zero = 0.236;% inches, undeformed diameter of tubes
Disp_initial = -0.08;
% Enter the mass of the payload
%mass=1; % lbf

%%%%%%%%%%%%%%%%%%%%%%%%%%%%%%%%%%%%%%%%%%%%%%%%%%%%%%%%%%%%%%%%%%%%%%%%
% SMA Tube Data
%%%%%%%%%%%%%%%%%%%%%%%%%%%%%%%%%%%%%%%%%%%%%%%%%%%%%%%%%%%%%%%%%%%%%%%%
% Material data presented here is for use with SMASIMTUBE.M
% Enter the initial temperature in degK:
%T = 100;

% Properties:
%C=1;% (slope in S-T space)
%MA=222;% First elastic stiffness
%MM=870;% Second elastic stiffness
%Tnload=[84 90 91 97.5]; % [Mof, Mos, Aof]
%etmax=0.115;% max uniaxial transformation strain
C=1;
MA=100;
MM=100;
Tnload=[84 91 90 97.5];
T=10000;
etmax=0.00010;

%%%%%%%%%%%%%%%%%%%%%%%%%%%%%%%%%%%%%%%%%%%%%%%%%%%%%%%%%%%%%%%%%%%%%%%%
% End of Data Input Section
%%%%%%%%%%%%%%%%%%%%%%%%%%%%%%%%%%%%%%%%%%%%%%%%%%%%%%%%%%%%%%%%%%%%%%%%

%%%%%%%%%%%%%%%%%%%%%%%%%%%%%%%%%%%%%%%%%%%%%%%%%%%%%%%%%%%%%%%%%%%%%%%%
% Initialize data for integration and material properties
%%%%%%%%%%%%%%%%%%%%%%%%%%%%%%%%%%%%%%%%%%%%%%%%%%%%%%%%%%%%%%%%%%%%%%%%
%fprintf('initializing constants, etc.\n');

% set up values for system and
% initial values of response and Material Parameters.
% simulation data is data needed by integration subroutine
simulation_data = [freq ymax number_top number_bot mass...
alpha gamma errorfactor T biasload Disp_initial Disp_initial];
% consists of:
% [frequency of excitation, amplitude of excitation,
% number of tubes for tension, number of tubes for compression,
% alpha constant, gamma constant, errorfactor constant
% ambient temperature]

% set up values of position values and material parameters

```

```

% for initial time step t=0
data(1,1:23) = 0;
t=0;

% data for time steps will be stored in the following
% arrays with the following format:
% [time position velocity acceleration y_displacement ...
% displacement1 force1 transformation_strain1 ...
% minimum_transformation_strain1 ...
% maximum_transformation_strain1 minimum_total_displacement1...
% maximum_total_displacement1 minimum_force1 ...
% maximum_force1 displacement2 force2 transformation_strain2 ...
% minimum_transformation_strain2 ...
% maximum_transformation_strain2 minimum_total_displacement2...
% maximum_total_displacement2 minimum_force2 maximum_force2]
%
% time = data(:,1)
% position of mass = data(:,2)
% velocity of mass = data(:,3)
% acceleration of mass = data(:,4)
% position of base = data(:,5)
%
% displacement of tube_top = data(:,6)
% value of force_top = data(:,7)
% transformation strain_top = data(:,8)
% minimum previous transformation strain_top = data(:,9)
% maximum previous transformation strain_top = data(:,10)
% minimum previous total displacement_top = data(:,11)
% maximum previous total displacement_top = data(:,12)
% minimum previous total force_top = data(:,13)
% maximum previous total force_top = data(:,14)
%
% displacement of tube2 = data(:,15)
% value of force2 = data(:,16)
% transformation strain2 = data(:,17)
% minimum previous transformation strain2 = data(:,18)
% maximum previous transformation strain2 = data(:,19)
% minimum previous total displacement2 = data(:,20)
% maximum previous total displacement2 = data(:,21)
% minimum previous total force2 = data(:,22)
% maximum previous total force1 = data(:,23)

straintp = [(C*(T-Tnload(2)))/MA (C*(T-Tnload(1)))/MM+etmax ...
(C*(T-Tnload(3)))/MM+etmax (C*(T-Tnload(4)))/MA];
stresstp = [C*(T-Tnload(2)) C*(T-Tnload(1)) C*(T-Tnload(3)) ...
C*(T-Tnload(4))];
m_data = [MA MM etmaxstraintp stresstp 1/etmax];

```

```

% Initialize tube data based on undeformed length and initial length

maxcount=100;
for i=1:maxcount
    strain0(i)= 0+(i-1)*Disp_initial/(maxcount-1);
end

for i=2:length(strain0)
    dstrain(i)=strain0(i)-strain0(i-1);
end
h_data = [0 0 0 0 0 0];
tstrainlast=0;

for i=1:(length(strain0))
    [sigsim(i), tstrain(i), h_data] = smasimtube(strain0(i), ...
        dstrain(i), tstrainlast, m_data, h_data);
    tstrainlast=tstrain(i);
end

data(1,6)=Disp_initial;
data(1,7)=sigsim(end);
data(1,8)=tstrain(end);
data(1,9:14)=h_data;
data(1,15:23)=data(1,6:14);

% initialize tubes based on mass to be isolated (account for gravity)
if init_for_g == 1

    sum_force = number_top*data(1,7)-number_bot*data(1,16);

    init_data_top=data(1,6:14);
    init_data_bot=data(1,15:23);

    delta = -0.00001;
    init_x = 0;

    while (biasload*mass >= -sum_force)
        init_data_top(1)=init_data_top(1)+delta;
        init_data_bot(1)=init_data_bot(1)-delta;
        [init_data_top(2), init_data_top(3), init_data_top(4:9)] = ...
            smasimtube(init_data_top(1), delta, ...
                init_data_top(3), m_data, init_data_top(4:9));

        [init_data_bot(2), init_data_bot(3), init_data_bot(4:9)] = ...
            smasimtube(init_data_bot(1), -delta, ...
                init_data_bot(3), m_data, init_data_bot(4:9));
        init_x=init_x+delta;
        sum_force = number_top*init_data_top(2)-...

```

```

    number_bot*init_data_bot(2);
end

data(1,6:14) = init_data_top;
data(1,15:23) = init_data_bot;
data(1,2) = init_x;

simulation_data(11) = Disp_initial+init_x;
simulation_data(12) = Disp_initial-init_x;
end

%%%%%%%%%%%%%%%%%%%%%%%%%%%%%%%%%%%%%%%%%%%%%%%%%%%%%%%%%%%%%%%%%%%%%%%%%%%%%%
% Begin Integration Routine
%%%%%%%%%%%%%%%%%%%%%%%%%%%%%%%%%%%%%%%%%%%%%%%%%%%%%%%%%%%%%%%%%%%%%%%%%%%%%%
fprintf('beginning integration\n');

while t < Time
tau2=tau;
[dataout, convergeflag] = nmstep_simple(t+tau2,...
tau2, simulation_data, data, m_data);
t=t+tau2;
data(end+1,:) = dataout;
end

return;

```

Newmark Integration Routine

The following code is the Newmark integration subroutine and is called by the system model. This code calls the simplified SMA pseudoelasticity model, described in Chapter III, in order to determine the force displacement response of the SMAs at the given timestep. This information is then used in the calculation of the mass position and returned to the system model.

```

function [dataout, convergeflag] = nmstep_simple(t,...
    tau, data_s, data_h, m_data);
% Newmark integration subroutine for simple model
% with variable time step
% data_s = [freq ymax number_tension number_compres mass alpha...
% gamma errorfactor temperature biasload disp_initial];
% data_h = [time position velocity acceleration y_displacement...

```

```

% displacement1 force1 transformation_strain1 ...
% minimum_transformation_strain1 ...
% maximum_transformation_strain1 minimum_total_displacement1...
% maximum_total_displacement1 minimum_force1 maximum_force1...
% displacement2 force2 transformation_strain2 ...
% minimum_transformation_strain2 ...
% maximum_transformation_strain2 minimum_total_displacement2...
% maximum_total_displacement2 minimum_force2 maximum_force2];
% m_data = material properties defined in input section
% dataout = current timestep data
% convergeflag = tells main program if integration converged
% retrieve simulation data from passing array
    frequency = data_s(1);
    amplitude = data_s(2);
    num_top = data_s(3);
    num_bot = data_s(4);
    mass = data_s(5);
    alpha = data_s(6);
    gamma = data_s(7);
    errorfactor = data_s(8);
    temperature = data_s(9);
    bias = data_s(10);
    disp0_top = data_s(11);
    disp0_bot = data_s(12);

% constants
%gconst = 32.2; % ft/s^2; accel of gravity

% retrieve time history of material
    x = data_h(end,2);
    xp = data_h(end,3);
    xpp = data_h(end,4);

    tube_top = data_h(end,9:14);
    tube_bot = data_h(end,18:23);

    tslast_top = data_h(end,8);
    tslast_bot = data_h(end,17);

    displast_top = data_h(end,6); %(x-y)
    displast_bot = data_h(end,15); %(x-y)

% create newmark weighting factors
    a1 = alpha*tau;
    a2 = (1-alpha)*tau;
    a3 = 2/(gamma*tau*tau);
    a4 = 2/(gamma*tau);
    a5 = 1/gamma-1;

```

```

err = 1;
xold = x;
tmp1 = a3;
tmp2 = (a3*x+a4*xp+a5*xpp);
tmp3 = xp+a2*xpp;
%%%%%%%%%%%%%%%%%%%%%%%%%%%%%%%%%%%%%%%%%%%%%%%%%%%%%%%%%%%%%%%%%%%%%%%%
% Begin Integration Routine
%%%%%%%%%%%%%%%%%%%%%%%%%%%%%%%%%%%%%%%%%%%%%%%%%%%%%%%%%%%%%%%%%%%%%%%%
i=0;
convergeflag = 1;
while (err > abs(xold*errorfactor))
    i=i+1;

    if i>20
        convergeflag = 0;
        dataout = [];
    return
end

    y = amplitude*sin(frequency*t*2*pi); %original forcing function

%disp1 = disp0+x-y; %tube 1 displacement
%disp2 = disp0+y-x; %tube 2 displacement

disp_top = disp0_top-x+y; %tube 1 displacement
disp_bot = disp0_bot-y+x; %tube 2 displacement

[F_top, tsc_top, tube_top_c] = smasintube(disp_top,...
disp_top-displast_top, tslast_top, m_data, tube_top);
[F_bot, tsc_bot, tube_bot_c] = smasintube(disp_bot,...
disp_bot-displast_bot, tslast_bot, m_data, tube_bot);

M = mass;
K = 0;
    F = num_top*F_top-num_bot*F_bot-mass*bias;

    Khat = K + M*tmp1;
    Fhat = F + M*tmp2;

    xold=x;

    x = Fhat/Khat;

    err = abs(x-xold);
end

```



```

    xpp = a3*x - tmp2;
    xp = tmp3 + a1*xpp;
dataout = [t x xp xpp y disp_top F_top tsc_top tube_top_c...
    disp_bot F_bot tsc_bot tube_bot_c];
return;

```

Plotting Routine

The following code allows the user to plot the various data gathered in the previous sections in an automated manner if the user does not wish to do so manually.

```

% Program to graph the data gathered running the
% vibration isolation simulation.

mass_values = [1.2];
tube_values = [2];
gload_values = [.1];
freq_values = [50:10:200];

transdata = zeros(length(freq_values),length(gload_values),...
length(tube_values),length(mass_values));
for i = 1:length(mass_values)
for j = 1:length(tube_values)
for k = 1:length(gload_values)

    filename = strcat('data\trans_m',....
    num2str(mass_values(i)), 't',...
    num2str(tube_values(j)),...
'g', num2str(k));
        load(filename)

        transdata(:,k,j,i) = trans;

        clear m t g f trans filename
    end
end
end

clear i,j,k

% plot trans vs f for given m and t

for i = 1:length(mass_values)
for j = 1:length(tube_values)

```

```

figure
plot(freq_values,transdata(:,1,j,i),...
      freq_values,transdata(:,2,j,i),...
      freq_values,transdata(:,3,j,i),...
      freq_values,transdata(:,4,j,i))
xlabel('frequency')
ylabel('transmittance')
titstr = ...
      strcat('effect of change in loading for mass = ',...
num2str(mass_values(i)), 'kg and tubes = ',...
num2str(tube_values(j)));
      title(titstr);

end

end

% plot trans vs f for given m and gload)
for i = 1:length(mass_values)
for j = 1:length(gload_values)

figure
plot(freq_values,transdata(:,j,1,i),freq_values,...
      transdata(:,j,2,i),freq_values,transdata(:,j,3,i))
xlabel('frequency')
ylabel('transmittance')
titstr = ...
      strcat('effect of change in tube count for mass = ',...
num2str(mass_values(i)), 'kg and gload = ',...
num2str(gload_values(j)));
      title(titstr);

end

end

% plot trans vs f for given tube and gload)
for i = 1:length(tube_values)
for j = 1:length(gload_values)

figure
plot(freq_values,transdata(:,j,i,1),freq_values,...
      transdata(:,j,i,2),freq_values,transdata(:,j,i,3))
xlabel('frequency')
ylabel('transmittance')
titstr = ...
      strcat('effect of change in mass for tube count = ',...
      num2str(tube_values(i)), ' and gload = ',...
      num2str(gload_values(j)));
      title(titstr);

```

end
end

VITA

John Jeremy Mayes, known as JJ by his friends, spent his formative years in the countryside near Cleveland, Texas. He is the son of George and Phyllis Mayes and has one sister, Mary. After graduating at the top of his high school class, he attended Texas A&M University earning a Bachelor of Science degree in aerospace engineering in 1999. He then decided to attend graduate school at Texas A&M University, again majoring in aerospace engineering and specializing in Shape Memory Alloys. He will leave university life to pursue a career with Bell Helicopter following completion of his Master's work. His permanent address is:

John Mayes

926 CR 2189

Cleveland, Tx 77327